Short Title

AN INVESTIGATION OF A HYDROSTATIC JOURNAL BEARING

AN INVESTIGATION OF AN EXTERNALLY PRESSURIZED HYDROSTATIC JOURNAL BEARING

by

C.R. Weldon, B.Eng. (Mech.) (McGill)

A thesis submitted to the Faculty of Graduate Studies
and Research in partial fulfilment of the requirements
for the degree of Master of Engineering

Department of Mechanical Engineering
McGill University
Montreal

July, 1971

ABSTRACT

A theoretical and experimental investigation of the behaviour of a 6in. diameter, 3-pocket hydrostatic journal bearing over a speed range of 0-1000 rpm. and a load range of 0-4000 lb. is described.

A theoretical model for the steady state operating characteristics of the bearing is presented. The effect of circulatory flow in the pocket is incorporated into expressions derived for frictional torque and lubricant temperature rise through the bearing.

The model also includes a quantitative assessment of the effect of variation of lubricant film thickness resulting from normal machining tolerances. It is shown that this variation can significantly distort the pressure profile in the bearing and thus affect related bearing characteristics.

Experimental results corroborate the theoretical prediction of the importance of circulatory flow and machining tolerances on bearing behaviour and show that classical theory yields an inadequate description of actual operational behaviour of high speed highly loaded hydrostatic journal bearings.

SUMMARY

An investigation of the operating characteristics of a 6in. diameter externally pressurized hydrostatic journal bearing is described. The journal was maintained in a position of zero eccentricity for the tests which were conducted through a speed range of 0-1000 r.p.m. and a load range of 0-4000 lb.

An over-relaxation process is used to obtain numerically the theoretical Laplacian pressure distribution over the bearing pad. Using this pressure distribution, expressions for the load capacity, flow rate and static film stiffness of the bearing are derived.

Circulatory flow of lubricant in the high pressure pockets is considered and an expression is developed for friction torque due to lubricant shear in the bearing which accounts for friction losses in the pockets due to the circulatory flow. It is shown that such friction losses in the pocket can be quite significant.

An expression for the temperature change of the lubricant through the bearing is developed which also takes account of lubricant circulation in the pocket. The results indicate that the commonly used procedure of taking the average film temperature as the arithmetic average between the inlet and outlet temperatures of the bearing can lead to large errors. The theory shows that the temperature rise in the pocket can be significant especially at low pocket pressures where the dwell time in the pocket is high. This results in the average temperature of the lubricant being closer to the outlet temperature than the arithmetic average, especially at low lubricant throughput.

The effect of machining tolerances upon bearing behaviour has been analysed. It is shown that the T.I.R. of the test bearing has values up to 25% of the film thickness. As predicted in the theory, and corroborated experimentally, the variation in film thickness produces hydrodynamic pressure peaks that are twice the magnitude of the pocket pressure. This results in increased torque loss and distortion of the temperature distribution in the bearing which significantly limits the worth of predicted bearing behaviour.

ACKNOWLEDGEMENTS

I wish to thank:

Dr. D. Atack for his guidance and encouragement throughout the project;

Mr. P.J. Zsombor-Murray for his assistance in the design of the experimental apparatus and the use of his test bed facilities;

Mr. L.J. Vroomen for his assistance on instrumentation;

Mr. D.C. Geller for his help in conducting the experiments;

Mrs. V. Read for typing the drafts and final copy of this thesis;

The Pulp and Paper Research Institute of Canada for the generous disposal of their services and facilities;

and the National Research Council for financial assistance.

TABLE OF CONTENTS

APPENDIX I

LIST OF FIGURES

LIST OF TABLES

x, y, z	Components in Cartesian coordinate system
X, Y, Z	Components of body force
u, v, w	Components of velocity
U	Journal surface velocity
R	Radius of bearing
D	Diameter of bearing
l	Representative length
h	Film thickness
H_o	Nominal radial clearance
A_o	Effective area of bearing pad
A	True area of bearing pad
A_l	Land area of bearing pad
V	Volume
P, p	Pressure
P_s	Source pressure
P_o	Pocket pressure
q	Volume flow rate

Q	Volume flow rate through bearing pad
Q_c	Circulatory flow
W	Load capacity
T	Torque
H_B	Power dissipation due to pressure energy conversion
H_{SL}	Power dissipation due to viscous shear over the land area
H_{sp}	Power dissipation due to viscous shear in the pockets
H_{pp}	Power dissipation due to pumping
$\bar{T}$	Temperature
$\bar{T}_I$	Lubricant inlet temperature
$\bar{T}_E$	Lubricant outlet temperature
K	Film stiffness
C_r	Resistive constant of bearing pad
r	Hydraulic resistance of bearing pad
$\bar{R}$	External resistance
c_p	Specific heat of lubricant at constant pressure
J	Joule equivalent
$\bar{D}$	Constant
B	Constant
a	Mesh length
n	Integer
θ, θ'	Angular measurement
α	Exponent factor in viscosity-pressure relationship

List of Symbols (cont'd)

α'	Relaxation factor
λ	Eigenvalue
ξ	Fractional constant
Ψ	Constant
τ	Shear stress
μ	Absolute viscosity of lubricant
μ_o	Absolute viscosity of lubricant at 100°F
ρ	Density of lubricant

INTRODUCTION AND STATEMENT OF THE PROBLEM

A recent investigation of the nip mechanics in a system consisting of two cylinders of different modulus running together in loaded rolling contact included measurements of rolling friction over a load range of 0-4000 lb. and a range of rotational speeds of 0-1000 r.p.m. The experimental method employed involved measurement of the total friction torque applied to the drive roll. This torque comprised both the rolling friction and the friction losses in the support bearings for the two rolls and it was found that the friction losses in the tapered-roller support bearings employed was of the same order of magnitude as the rolling friction between the cylinders (1). To obtain accurate values of the rolling friction it was necessary to measure the friction losses in the support bearings as a function of load and rotational speed by independent dynamometry. Agreement between the measured values and those predicted from Palmgren's empirical equations for the friction losses in such bearings (2) was quite poor, particularly at low rotational speeds. This was not entirely surprising for although the nature of the dissipative mechanism in a roller bearing is well understood, no satisfactory quantitative theory for the prediction of friction losses exists. It was concluded that accurately predictable values of friction losses in roller bearings could not be obtained. Thus, in continuing studies of the type described, where interest centres around an accurate measurement of only part of the total friction loss and that part cannot be easily isolated, it would be necessary to resort to independent and often inconvenient measurement of the friction torque of the support bearings.

One possible alternative would be to use another type of support bearing whose friction losses could be predicted with the requisite accuracy over the full load and speed range. Hydrostatic journal bearings seem attractive not only in this regard, but also for the application under investigation have the added attraction of high stiffness.

Hydrostatic bearings have been employed almost invariably for the support of extremely heavy loads moving at low speeds and their use in relatively high-speed applications has only recently been contemplated. Thus, it was decided to conduct a study of hydrostatic journal bearing behaviour over a range of loads and rotational speeds of 0-4000 lb. and 0-1000 r.p.m. respectively in an attempt to satisfy the above requirements and also for its own intrinsic value. The main aspects of current theory of hydrostatic journal bearing behaviour will first be examined and the theory will be supplemented or modified where it does not adequately explain the operational behaviour at high-speeds. The resulting theory will then be tested experimentally.

A typical hydrostatic journal bearing, shown schematically in Fig.1, consists of one or more hydrostatic thrust bearings arranged in circular array around a journal.

The one shown consists of three bearing pads symmetrically disposed at 120° around the inner circumference of the bearing. Each pad has three main parts - a land or sill area, a pocket or recess area which acts as the reservoir for high pressure lubricant and a lubricant inlet. The pads may be isolated from each other by axial pressure reliefs which separate adjacent axial lands. The land area around the pocket, in this case rectangularly shaped, consists of two axial and two circumferential segments. Radial

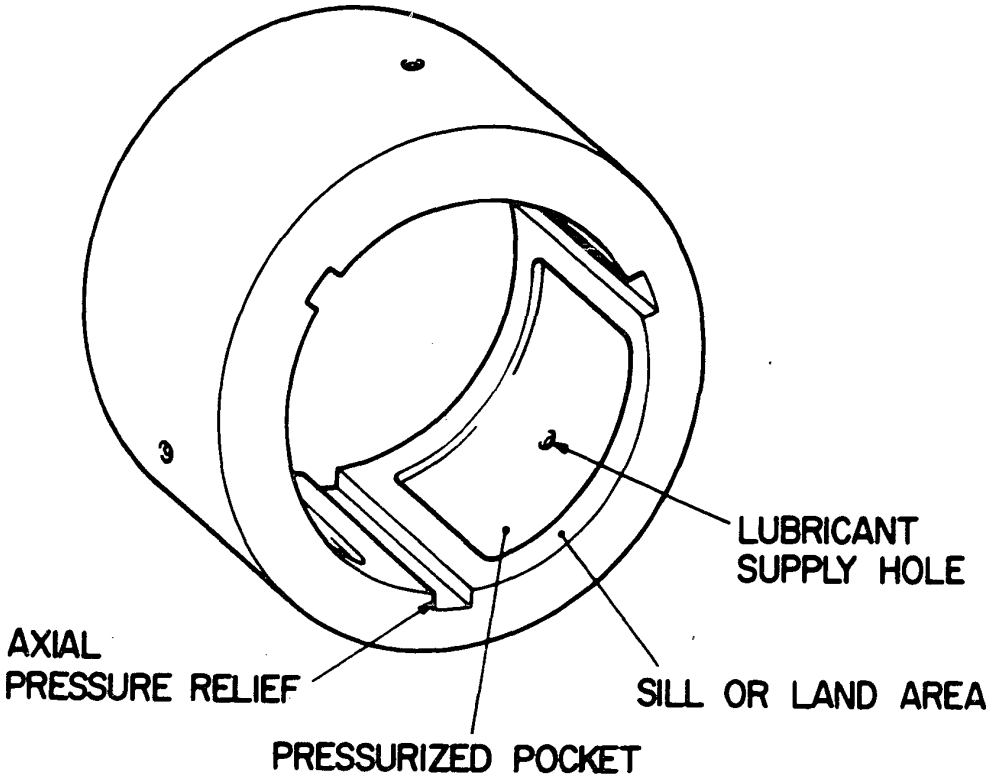

FIG. 1.

clearance between the journal and the land is typically of the order of 0.001 - 0.01 in. and the pocket depth is generally 50 - 100 times the radial clearance. Pressurized fluid flows into the bearing through a lubricant inlet which is centrally disposed in the base of the pocket. Proper operation of the bearing demands that a full-fluid film be maintained over the land area at all times. This requires, amongst other things, a continuous supply of lubricant to the pocket at a pressure sufficiently high to support the radial loading of the journal. The pressurized lubricant supply system normally comprises a pump, a lubricant collection and recirculation system, a filter system and a temperature regulated lubricant cooling system to ensure that lubricant is supplied

to the bearing at the desired temperature and viscosity.

Probably the earliest demonstration of the principles of hydrostatic lubrication was given in a novel and popular exhibit at the Paris International Exhibition of 1878. These principles have, only recently, been developed to any appreciable extent for use in practical bearings. Fuller (3) published a series of articles in 1947 in which certain basic principles of bearing design were established and several possible applications discussed. Since that time many hydrostatic bearings have been designed for a large variety of applications, mainly for the support of large slowly moving loads, as for example, the support bearing for the Hale 200in. optical telescope on Mount Palomar (4).

More recently, Rippel (5) published a design manual in which all the salient operating aspects of low-speed hydrostatic bearings are discussed. Rippel observes that little is known about the effects of journal rotation on the hydrostatic pressure field, and hence on the resulting performance of hydrostatic journal bearings, apart from the fact that lubricant temperature will increase and lubricant viscosity will decrease with increasing speed.

Royle, Howarth and Caseley-Hayford (6) describe an automatic flow valve for maintaining the journal in a concentric attitude in a hydrostatic journal bearing operating at rotational speeds through the range 0-1200 r.p.m. and supporting loads of up to 320 lb. Their experimental data show that under these conditions the friction torque is substantially independent of load and directly proportional to rotational velocity. Theoretical predictions of torque, presumably calculated according to Petroff's equation (7), were found to agree quite well with the measured values.

These results provided an encouraging stimulus to the solution of the dynamometry problem already outlined, the only question being whether the predicted dependence of torque on load and speed remains unchanged at loads of up to 4000 lb.

The authors did not anticipate any large change in friction torque when the bearing was required to support higher loads. However, they did insert a note of caution to the effect that should surface irregularities become significant in comparison with the mean radial clearance, or should tilt occur, causing the intrusion of hydrodynamic effects, large changes in the pressure distribution in the lubricant film would occur and bearing performance would be affected. In this latter regard Rippel (5) gives a rule of thumb to be followed regarding allowable dimensional tolerances; geometrical irregularities in the surfaces of the journal and the bearing should be sufficiently small that the variation in lubricant film thickness does not exceed 30% of the mean film thickness over the bearing land areas.

Shinkle and Hornung (8) have given a theoretical and experimental analysis of the friction torque in a high-speed hydrostatic journal bearing in which it is shown that a significant contribution to the friction torque can arise from shearing the lubricant in the bearing pockets as the journal speed increases. In the derivation of the expression for the friction torque it is shown that a linear pressure gradient, whose magnitude is proportional to the journal speed, is set up along the length of the pocket in the circumferential direction. This gradient gives rise to circulation of lubricant in the pocket, and causes pressure spikes at the ends of the pocket due to inertial effects associated with reversal of the direction of lubricant flow at these points. No estimate of the magnitude of these

pressure spikes is given. At high rotational speeds the friction loss in the pocket is comparable to the friction loss over the land, and when the flow in the pocket becomes turbulent the pocket friction loss may exceed that over the land. Experimental data agree quite well with theoretical predictions though, as in the studies of Royle et al, the load was quite low, being only 75 lb. In developing the expression for friction torque it was assumed that axial flow of lubricant from the pocket was negligible compared with circumferential flow. This assumption becomes less valid as the load, and hence the hydrostatic pressure in the pockets required for support, is increased.

In all these studies it has been assumed that the pressure distribution in the lubricant film is Laplacian, whatever the operating eccentricity. Raimondi and Boyd (9) present experimental data relating load and flow-rate factors to a bearing design parameter for a hydrostatic journal bearing operated at various eccentricities. Agreement between experiment and theory is poor, pointing to the inadequacy of the assumption of a Laplacian pressure distribution existing over the bearing land area for any but concentric operation.

A series of articles by O'Donoghue and Rowe (10) on hydrostatic bearing design based on an 'exact solution of the Laplace equation under non-uniform film conditions' was published shortly after the experimental phase of the present study was completed. The case of a four pocket hydrostatic journal bearing operating at various values of the eccentricity is treated and the predicted shape of a typical pressure profile set up in the fluid film is given. Unfortunately, it bears little resemblance to the pressure profiles measured in this study.

Dickson (11) presents a simplified approach for the derivation of load capacities in the turbulent flow regime, in which the possibility of hydrodynamic effects due to journal rotation at eccentricities above zero is ignored. The experimental data show deviations of about 30% from the theoretical predictions.

Bearing performance is profoundly affected by small changes in lubricant temperature and surprisingly, scant reference can be found in the literature to investigations on the temperature distribution in the lubricant film in a hydrostatic bearing. The only reference to such an investigation which could be found is one published recently by Kher and Cowley (12). It deals with the temperature effects in a 2in. diameter hydrostatic journal bearing at journal speeds of up to 1900 r.p.m., without external loading. They measured circumferential and radial temperature gradients in the bearing and the temperature of the oil film along the bearing circumference. In the present study, where higher loads have been employed, it may be expected that the temperature gradients in the oil through the bearing would be larger and, in view of the large non-linear temperature coefficient of viscosity of normal lubricating oils (13), would have a more pronounced effect on the bearing behaviour.

In the treatment of temperature effects in other fluid-film bearings, including low-speed hydrostatic bearings, the assumption is often made that the temperature of the lubricant is the average of the inlet and outlet temperatures. If the difference between these two temperatures is small, as is the case for bearings operated at low speeds, the assumption proves to be reasonably good. However, when the temperature difference is large, as may be expected in high-load, high-speed bearings, the assumption is of

doubtful value, particularly when it is noted that a change of temperature of 1°F corresponds to a change of about 10% in the viscosity of the lubricant in the normal operating temperature range. A useful guide to the magnitude and nature of these changes may be obtained by reference to papers by Cole (14), Hagg (15) and Muscat and Morgan (16) who have considered the temperature distribution in the lubricant film in a high speed, highly loaded journal bearing.

There is a large number of theoretical treatments in the literature which deal with the stability characteristics of low speed hydrostatic bearings. Admittedly, the inherent stability of a hydrostatic bearing is its most attractive feature, but there would appear to be little point in studying this parameter further in the present context until other more basic operating parameters of the bearing such as the variation of pressure and temperature in the lubricant film are accurately predictable. Existing theory of hydrostatic bearing behaviour has not received adequate experimental confirmation for high speed, high load operation.

The present experiments were performed on a 6in. diameter hydrostatic journal bearing. The bearing has three pockets completely surrounded by close clearance lands separated from the adjacent pockets by axial pressure reliefs as shown in Fig. 1.

Circumferential pressure profiles in the central plane of the bearing were measured. These show that the influence of normal machining tolerances on the pressure profile is very marked and that even when the bearing is running at zero eccentricity it cannot be assumed that a Laplacian pressure distribution exists.

Measured friction torques display wide divergences from those predicted by Petroff's equation. These divergences cannot be wholly explained by making a correction for pocket friction losses, but appear to result, in part, from the pressure profile distortion caused by variations in the lubricant film gap due to dimensional tolerances.

Temperature measurements on the bearing indicate the inadequacy of the assumption that the average temperature of the lubricant in the bearing is the average of the inlet and outlet temperatures of the lubricant. A theory is developed which considers the lubricant dynamics in the pocket as well as over the lands and provides a much better estimate of average lubricant temperature.

In conclusion, agreement of measured results with the predictions of classical theory is poor. Improvements in the theory, made in this study, provide a much better estimate of high speed, high load bearing performance since they take account of effects which occur in real bearings.

THEORETICAL

The first step to be taken in the theoretical analysis of hydrostatic bearing performance is to derive a fluid dynamic model for the bearing pads from which the distribution of pressure in the support film can be obtained. Load and flow coefficients describing bearing performance can then be predicted.

Continuous film lubrication is described by a particular form of the Navier-Stokes equations known as Reynold's equation. Among the parameters in Reynold's equation is the fluid-film thickness, and if this is constant, as is usually the case for a hydrostatic bearing, Reynold's equation reduces to Laplace's equation. There is no closed analytical solution of Laplace's equation for the rectangular bearing-pad configuration considered in this study and it is necessary to resort to a numerical solution.

The load capacity is then determined for any arbitrary value of the inlet pressure by numerical evaluation of the appropriate integral involving the calculated pressure distribution at that inlet pressure and the bearing pad area. This may be expressed as the product of the inlet pressure and an effective bearing pad area. Load capacity for any value of inlet pressure for this pad configuration is determined as the product of this effective bearing pad area and the inlet pressure.

Flow rate is derived by numerical evaluation of the resistance to flow in the bearing pad, and is obtained from an analysis of the pressure distribution.

Also included are theoretical derivations of bearing friction loss

due to lubricant shear, the temperature change of the lubricant as it passes through the bearing, stiffness characteristics of the bearing and the influence of bearing tolerances on the idealised Laplacian pressure distribution.

Derivation of the Pressure Field

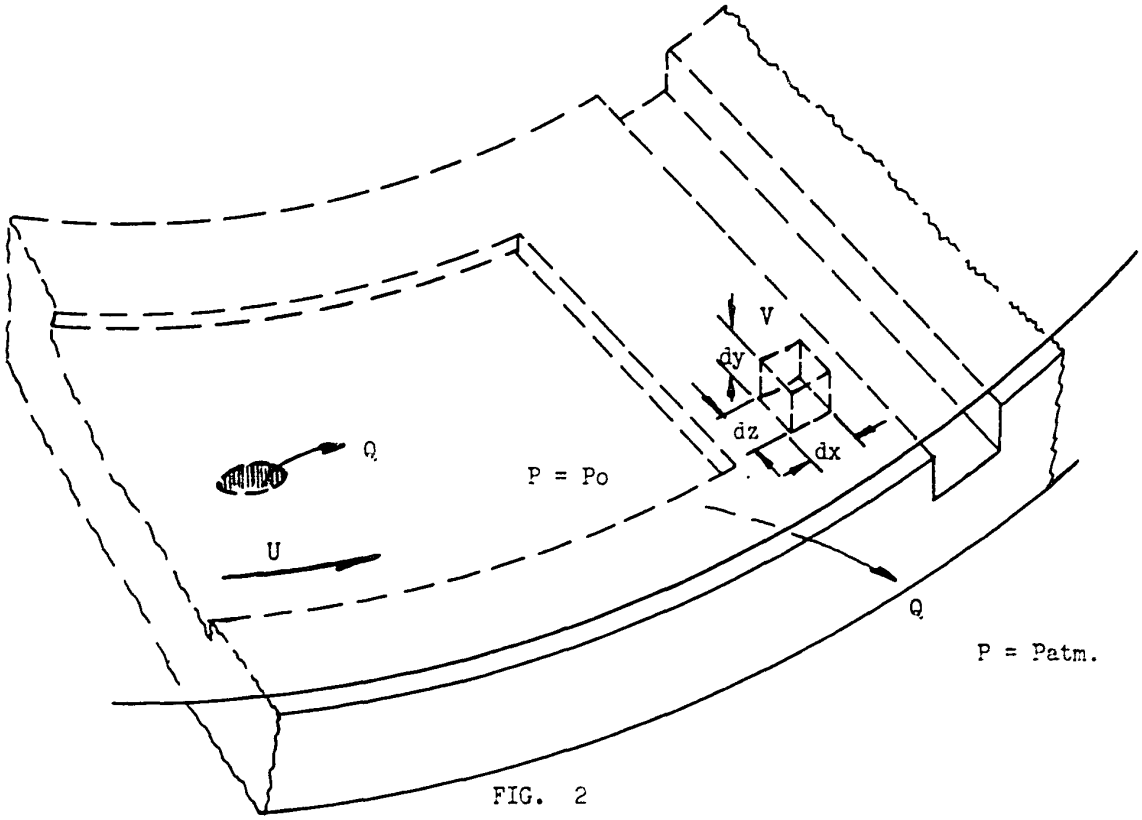

FIG. 2

Schematic drawing showing part of a hydrostatic journal bearing in the neighbourhood of a pressure pad. A volume element on the sill area is considered for the analysis of the pressure distribution.

Consider a small arbitrary volume element, V, between the land and the journal where the fluid is flowing from the pocket over the land to the atmosphere as shown in Fig. 2. Let the pocket pressure be Po and the velocity of the journal surface be U.

Assuming that the fluid behaves in a Newtonian manner, pressure and shear forces in the x direction of the fluid element are as shown in Fig. 3.

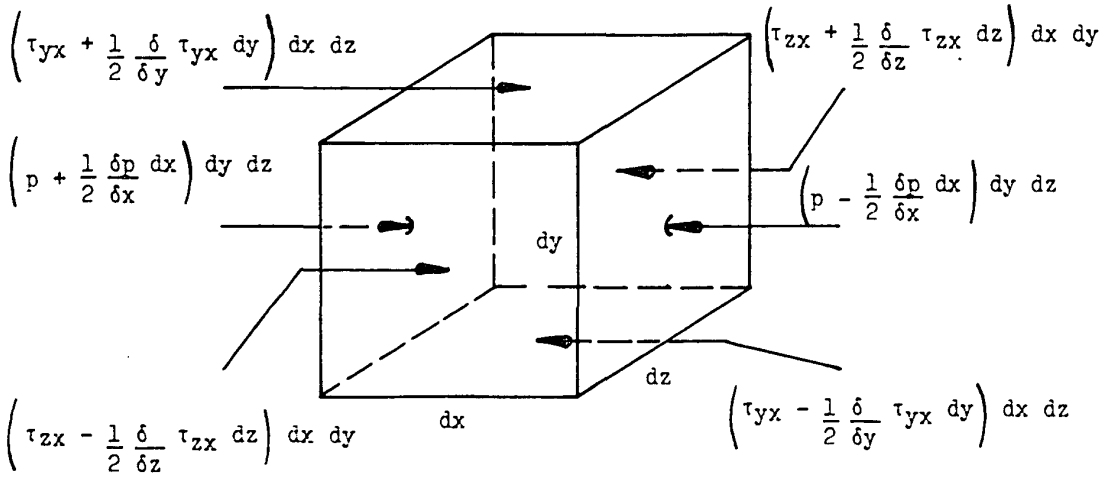

FIG. 3

Forces acting in the x direction on the surfaces of a fluid element. All stresses are a function of position. At the centre of the element the pressure is p and the shear stresses τ_{yx} and τ_{zx}.

From a consideration of these forces, in addition to inertial and body forces, an equation of motion for the viscous fluid in the x direction can be obtained. General equations of motion, the Navier-Stokes equations, for a viscous fluid element V, may be written in the following form (17):

X-momentum

$$\rho \frac{Du}{Dt} = \rho X - \frac{\delta p}{\delta x} + \frac{2}{3} \frac{\delta}{\delta x} \mu \left(\frac{\delta u}{\delta x} - \frac{\delta w}{\delta z} \right)$$

$$+ \frac{2}{3} \frac{\delta}{\delta x} \mu \left(\frac{\delta u}{\delta x} - \frac{\delta v}{\delta y} \right) + \frac{\delta}{\delta y} \mu \left(\frac{\delta u}{\delta y} + \frac{\delta v}{\delta x} \right) \qquad - (1a)$$

$$+ \frac{\delta}{\delta z} \mu \left(\frac{\delta w}{\delta x} + \frac{\delta u}{\delta z} \right)$$

Y-momentum

$$\rho \frac{Dv}{Dt} = \rho Y - \frac{\delta p}{\delta y} + \frac{2}{3} \frac{\delta}{\delta y} \mu \left(\frac{\delta v}{\delta y} - \frac{\delta u}{\delta x} \right)$$

$$+ \frac{2}{3} \frac{\delta}{\delta y} \mu \left(\frac{\delta v}{\delta y} - \frac{\delta w}{\delta z} \right) + \frac{\delta}{\delta z} \mu \left(\frac{\delta v}{\delta z} + \frac{\delta w}{\delta y} \right) \qquad - (1b)$$

$$+ \frac{\delta}{\delta x} \mu \left(\frac{\delta v}{\delta x} + \frac{\delta u}{\delta y} \right)$$

Z-momentum

$$\rho \frac{Dw}{Dt} = \rho Z - \frac{\delta p}{\delta z} + \frac{2}{3} \frac{\delta}{\delta z} \mu \left(\frac{\delta w}{\delta z} - \frac{\delta u}{\delta x} \right)$$

$$+ \frac{2}{3} \frac{\delta}{\delta z} \mu \left(\frac{\delta w}{\delta z} - \frac{\delta v}{\delta y} \right) + \frac{\delta}{\delta x} \mu \left(\frac{\delta w}{\delta x} + \frac{\delta u}{\delta z} \right) \qquad - (1c)$$

$$+ \frac{\delta}{\delta y} \mu \left(\frac{\delta w}{\delta y} + \frac{\delta v}{\delta z} \right)$$

where $\frac{D}{Dt} = \frac{\delta}{\delta t} + u \frac{\delta}{\delta x} + v \frac{\delta}{\delta y} + w \frac{\delta}{dz}$

and u, v, w are the velocity components of the fluid in the x, y, z coordinates respectively, ρ is the density and μ the viscosity of the fluid.

Terms on the left are the inertia terms and those on the right are

due to body force, pressure and viscous shear respectively.

These momentum equations can be greatly simplified for the present application by making an order of magnitude analysis. Typically, the fluid film thickness is three or four orders of magnitude smaller than a land dimension, therefore, only derivatives of velocity gradients in the y direction need be considered. Further, full-fluid film lubrication generally operates in the region of laminar flow implying that v = o. If l is a representative dimension of the bearing pad and h is the fluid film thickness, the pressure gradient $\delta p/\delta y$ is h/l times smaller than the pressure gradients in the x and z directions and may therefore be neglected. Finally, if the effect of body forces, such as gravity, and acceleration forces such as centrifugal forces associated with the movement of lubricant along a circular path are neglected, the Y-momentum equation is eliminated and the X and Z -momentum equations reduce to:

$$\frac{\delta p}{\delta x} = \frac{\delta}{\delta y} \mu \left(\frac{\delta u}{\delta y} \right)$$

$$\frac{\delta p}{\delta z} = \frac{\delta}{\delta y} \mu \left(\frac{\delta w}{\delta y} \right) \qquad - (2)$$

Assuming that viscosity is a function of temperature only, equations (2) may be integrated to obtain the velocity components. Substituting these into the continuity equation and assuming that the fluid density is constant we obtain Reynold's equation.

For example, the first of equations (2) may be written:

$$\frac{\delta^2 u}{\delta y^2} = \frac{1}{\mu} \left(\frac{\delta p}{\delta x} \right)$$

Integrating twice and observing the following boundary conditions

$$u = o, \quad u = U.$$

$$y = o, \quad y = h.$$

$$u = \frac{1}{2\mu}\left(\frac{\delta p}{\delta x}\right) y\,(y-h) + \frac{y}{h}\,U$$

For w the boundary conditions are:

$$w = o, \quad w = o.$$

$$y = o, \quad y = h.$$

Therefore: $$w = \frac{1}{2\mu}\left(\frac{\delta p}{\delta z}\right) y\,(y-h)$$

Substituting in the continuity equation:

$$\frac{\delta(\rho u)}{\delta x} + \frac{\delta(\rho w)}{\delta z} = 0$$

where ρ is constant. Integrating between $y = o \rightarrow h$ we obtain:

$$\rho \int_o^h \frac{\delta}{\delta x}\left[\frac{1}{2\mu}\left(\frac{\delta p}{\delta x}\right) y\,(y-h) + \frac{y}{h}\,U\right] dy + \rho \int_o^h \frac{\delta}{\delta z}\left[\frac{1}{2\mu}\left(\frac{\delta p}{\delta z}\right) y\,(y-h)\right] dy = 0$$

which simplifies to Reynold's equation:

$$\frac{\delta}{\delta x}\left[h^3\left(\frac{\delta p}{\delta x}\right)\right] + \frac{\delta}{\delta z}\left[h^3\left(\frac{\delta p}{\delta z}\right)\right] = 6\,U\mu\,\frac{dh}{dx} \qquad - \quad (3)$$

Since this investigation deals mainly with the operation of a bearing operating at zero eccentricity, the fluid film thickness, h, is constant and $dh/dx = o$. Assuming additionally that μ is the viscosity of the lubricant at the average temperature of the fluid film and does not vary in the direction of flow, Reynold's equation reduces to Laplace's equation:

$$\frac{\delta^2 p}{\delta x^2} + \frac{\delta^2 p}{\delta z^2} = 0 \qquad - (4)$$

In spite of these simplifications there is no closed analytical solution of equation (4) for the general case of a rectangular pad with a rectangular recess.

The following numerical solution is relatively simple, economical and can yield design curves for bearing characteristics for a wide range of pad geometries.

Numerical Solution of Laplace's equation

A numerical solution is effected by superimposing on the pad geometry a square mesh such as shown in Fig. 4. Because of symmetry considerations only one quarter of the pad need be investigated. An estimated pressure value is inserted at each nodal point and these are modified to satisfy the finite difference form of Laplace's equation:

$$P_A + P_B + P_C + P_D - 4P_O + O(a^2) = 0 \qquad - (5)$$

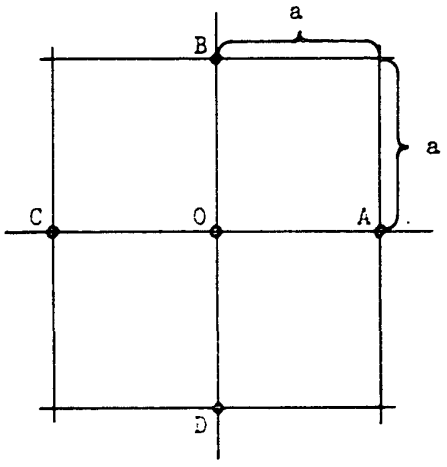

FIG. 4

P_A, P_B, P_C, P_D and P_O are pressures at A, B, C, D and O and a is the mesh unit. Terms in (a^2) and those of higher order are neglected.

The problem is reduced to solving a set of simultaneous equations, one for each nodal point. In general equation (5) will not be satisfied exactly and there will be a residual given by

$$\Delta P_0 = P_A + P_B + P_C + P_D - 4P_0 \qquad - (5a)$$

The process of relaxation or, in this case, over-relaxation provides a mechanism for reducing these residuals to zero.

After applying equation (5a) to point 0, Po is corrected to a value

$$P_0^{n+1} = P_0^{n} + \Delta P_0^{n} \cdot \alpha'$$

where α' is an over-relaxation constant and has a value between 0 and 2, normally 1.6.

The inclusion of a relaxation factor is important when settling a display on a rectangular bearing pad since the sharp corners give rise to errors which propagate throughout the mesh and decay slowly. The over-relaxation technique provides a method for over-correcting the residual at every nodal point and can improve the settling time for the display by a factor of 30. The optimum value of α' can be found from the relationship.

$$\alpha' \text{ opt.} = 2/ [1 + (1 - \lambda)^{\frac{1}{2}}]$$

where λ is the largest eigenvalue of the display matrix.

Treatment of the Boundary Conditions

For the case of a hydrostatic pad the boundary conditions on the inner and outer edges are usually constant. They are not corrected by equation (5a) but are used in correcting adjacent points. Nodal values on the symmetry lines are not boundary values and therefore are worked out with a slight

modification. Taking advantage of symmetry as seen in Fig. 5, equation (5a) becomes:

$$\Delta P_o = P_A + 2P_B + P_C - 4P_O$$

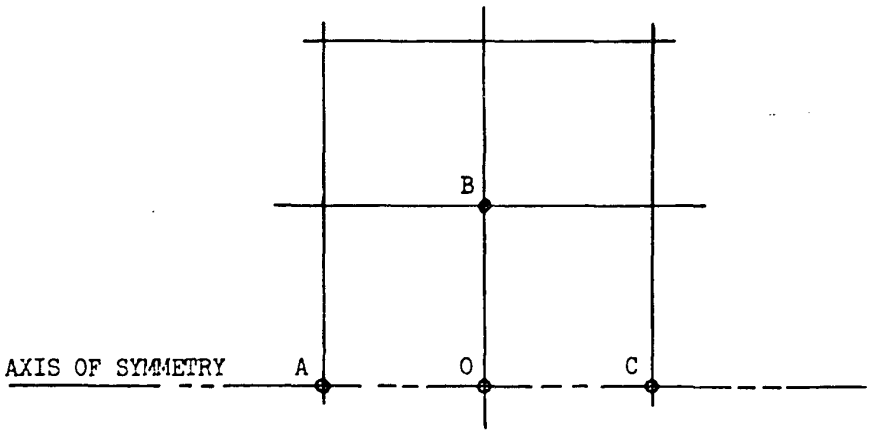

FIG. 5

Finally for the case where the grid cannot be made to fit the boundaries as shown in Fig. 6 we have for equation (5a):

$$\Delta P_o = 2P_A/\xi(1+\xi) + 2P_C/(1+\xi) + P_B + P_D - 2(1+1/\xi)P_C$$

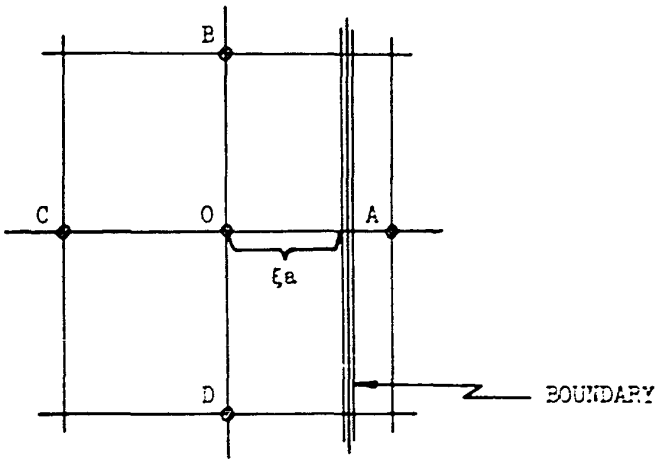

FIG. 6

Fig. 7, which is given in Appendix 1, shows the computer programmes used for settling the pressure fields for both the projected and developed pads. Figs. 8 and 9 show typical settled fields for one quadrant of the projected and developed bearing pads respectively, computed for an inlet pressure of 1000 p.s.i. It will be appreciated that the field for each pad is geometrically similar for different values of the inlet pressure and differs only in magnitude.

Load Capacity

The load capacity of a hydrostatic journal bearing is a function of inlet pressure and bearing pad geometry. It is an important parameter of bearing performance since the primary function of a bearing is to support a load.

The load capacity, W, is defined as the integral of the pressure over the total projected bearing pad area. It may also be defined in terms of the pocket pressure as shown in the following equation:

$$W = \int P \, dA = P_o A_o \qquad - (8)$$

where Ao is defined as the effective bearing pad area or that area which will support the same load as the bearing, assuming the pressure to be constant and equal to the pocket pressure acting over the effective area.

Thus, the effective bearing pad area is a constant fraction of the total bearing pad area for a given pad geometry and

$$A_o = K A \qquad - (9)$$

K can be found by substituting (9) into (8) as follows:

$$K = \frac{\int P \, dA}{P_o A} = \int_{\text{area}} \frac{P \, dA}{P_o A} \qquad - (9a)$$

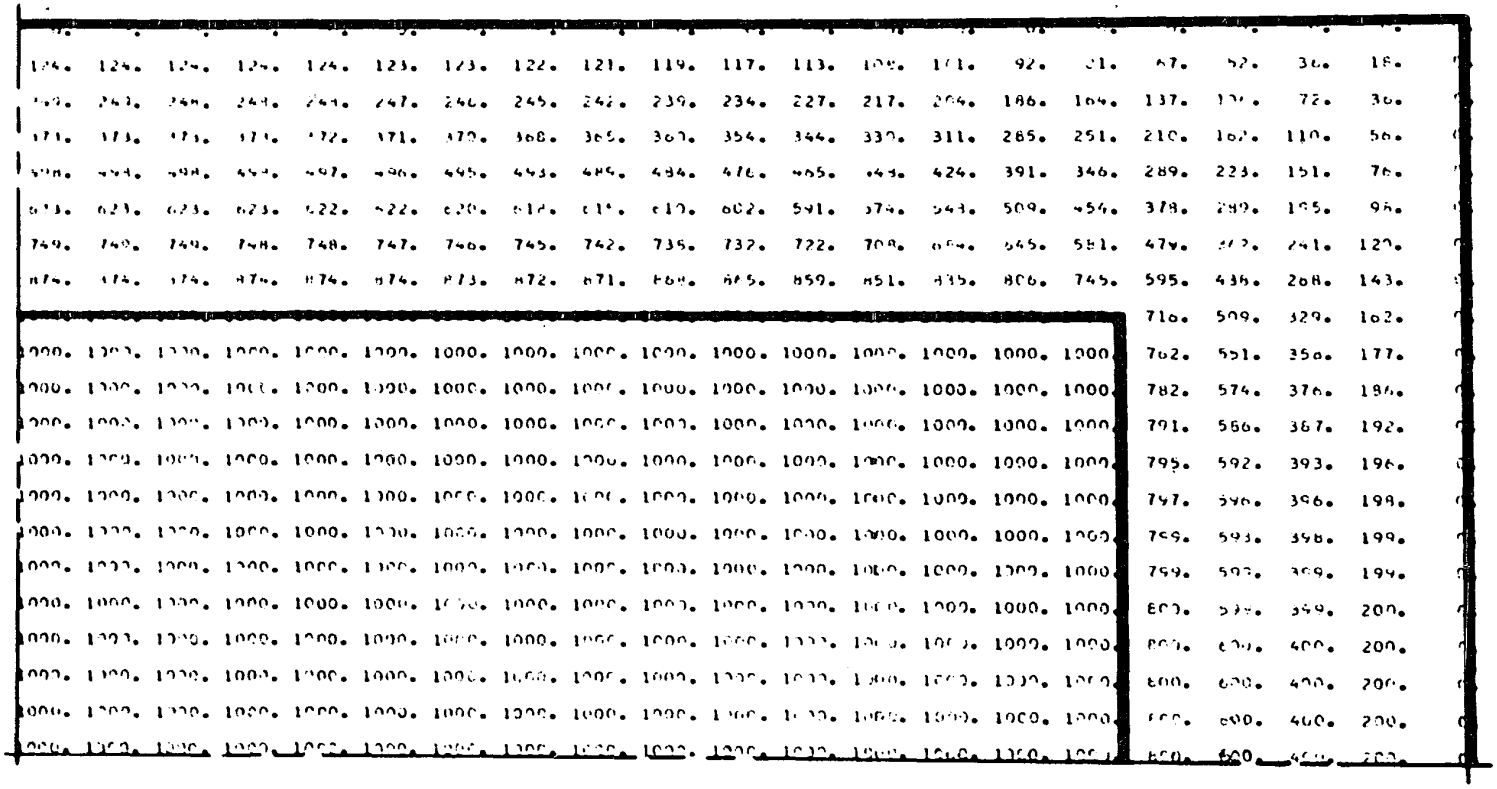

FIG. 8

Represents the Laplacian pressure distribution over one quadrant of the projected bearing pad assuming a pocket pressure of 1000 p.s.i.g. and an exhaust pressure of 0 p.s.i.g. The effective bearing pad area obtained from this pressure distribution is used to obtain the load capacity of the bearing pad.

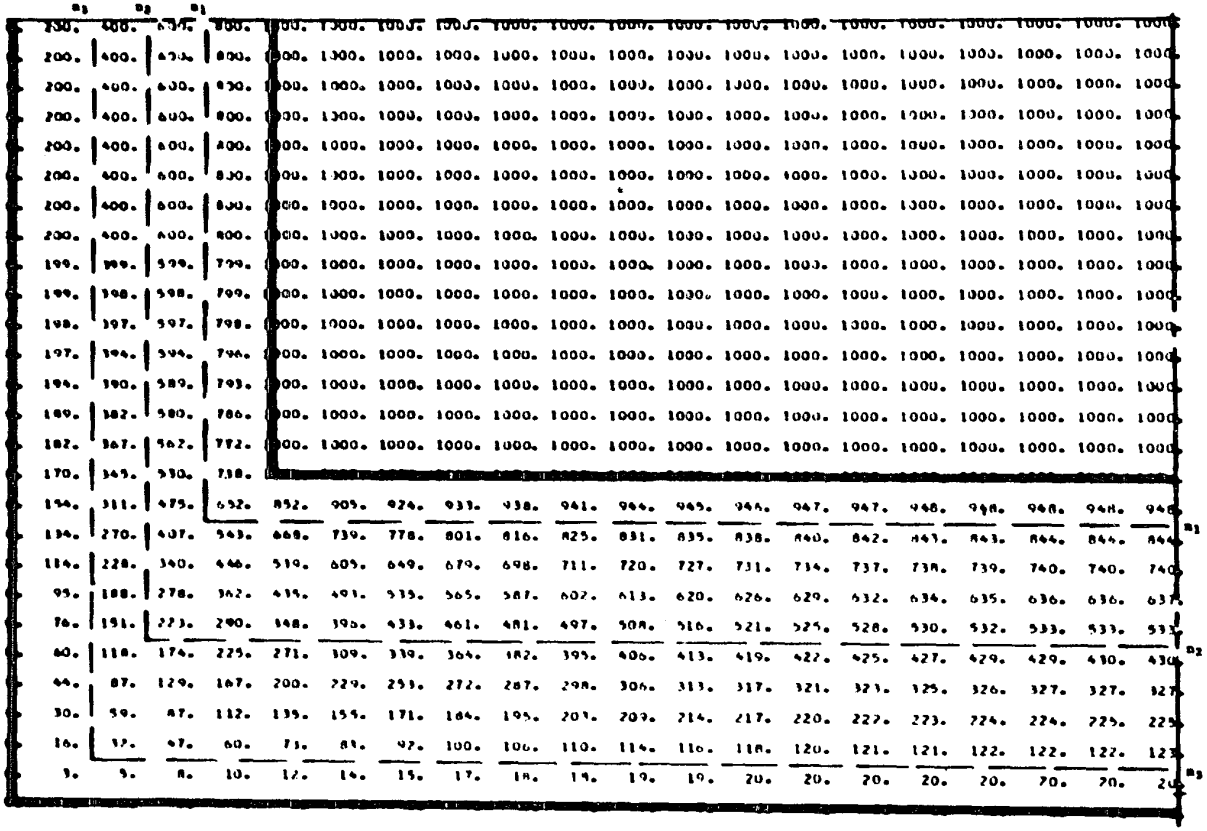

FIG. 9

Represents the Laplacian pressure distribution over one quadrant of the developed bearing pad, assuming a pocket pressure of 1000 p.s.i.g. and an exhaust pressure of 0 p.s.i.g. Three contour lines n_1, n_2 and n_3 are arbitrarily chosen to obtain three independent values of the resistive constant, C_r, of the bearing pad. This constant is used to calculate lubricant flow rates over the land areas of the bearing pad.

This can be evaluated numerically. Since the solution to Laplace's equation is computed on a grid of constant mesh length a, all area elements dA of equation (9a) equal a^2 and can be taken outside the sum. Further, A/dA is the total area of the pad divided by the unit mesh area, and is equivalent to the total number of grid squares. Therefore:

$$K = \frac{\Sigma P_n}{P_o \times n} \qquad - (9b)$$

where P_n is the pressure at the nth nodal point and n is the number of grid squares.

It is only necessary to sum the pressures in a symmetrical quarter of the bearing pad using half-values on the symmetry lines and a quarter-value at the centre.

Fig. 8 represents a typical Laplacian pressure display, on a (21, 21) matrix, on a symmetrical quarter of one of the bearing pads in projected area, for an inlet pressure of 1000 psi assuming the peripheral pressure to be zero. Using equation (9b) and taking data from Fig. 8, $\Sigma P_n = 275{,}123$, $n = 20 \times 20$:

$$K = \frac{275{,}123}{1000 \times (20 \times 20)} = 0.687$$

The true pad area is 18.40 sq.in. and the effective area is therefore:

$$A_o = K.A = 0.687 \times 18.40 = 12.65 \text{ sq.in.}$$

The general equation for the load capacity of the test bearing is:

$$W = P_o \times A_o = 12.65 \times P_o \text{ lb.}$$

and for $P_o = 1000$ psi

$$\underline{W = 12{,}650 \text{ lb.}}$$

Flow Rate

An essential requirement of a hydrostatic bearing is that a full fluid film be maintained between the journal and the bearing sills at all times. It is therefore necessary to know how much lubricant must be supplied to the bearing to achieve this. Flow rate, Q, is defined as the volume throughput of lubricant necessary to maintain a load supporting film. It depends upon inlet pressure, film resistance and the physical properties of the lubricant.

An expression for flow rate can be derived by integrating equations (2) twice and observing the following boundary conditions

$$y = o, \quad u = o, \quad w = o.$$
$$y = h, \quad u = U, \quad w = o.$$

to obtain the velocities u and w as previously derived. These expressions are then integrated again across the thickness of the fluid film and the following expressions are obtained for flow rate.

$$q_x = -\frac{h^3}{12\mu}\left(\frac{\delta p}{\delta x}\right) + \frac{h}{2}(U) \qquad - (10)$$

$$q_z = -\frac{h^3}{12\mu}\left(\frac{\delta p}{\delta z}\right)$$

The term hU/2 is the shear flow due to journal rotation while the terms containing a pressure gradient represent pressure flow.

In the flow rate expression we are only interested in the pressure flow, that is the amount of flow which must be supplied to the bearing pad by a pump. Shear flow can be ignored. Combining equations (10) we get for total pressure flow

$$Q = (q_x^2 + q_z^2)^{\frac{1}{2}} = \frac{h^3}{12\mu} \oint_n \left(\frac{\delta p}{\delta l}\right) \cdot dn \qquad - (11)$$

where $\delta p/\delta l$ is the pressure gradient normal to any closed contour n. Equation (11) is often written in the form:

$$Q = \frac{h^3}{C_r} \cdot \frac{Po}{\mu} \qquad - (12)$$

where

$$C_r = \frac{12\ Po}{\oint_n \left(\frac{\delta p}{\delta l}\right) \cdot dn} \qquad - (13)$$

where C_r is termed the resistive constant of the bearing.

Fig. 9 shows a typical settled pressure field on the developed pad for an inlet pressure of 1000 psi and a peripheral pressure of zero. Three suggested contour lines are shown for the summing procedure. Using contour 2, for example, pressure differences are summed along the contour using half values on the symmetry lines. The value 223 at the inside of the corner is used twice and the value 118 diagonally opposite is ignored. We have then:

$$4 \times \sum_{n_2} \left(\frac{\Delta p}{\Delta l}\right) = 5300 \text{ p.s.i.} \qquad - (14)$$

Therefore:

$$C_r = \frac{12 \times 1000}{5300} = 0.566$$

An indication of the accuracy obtained by using a grid of this coarseness can be seen by computing values of C_r from the other two contours shown. All values differ only in the fourth decimal place.

Stiffness

It has been implicitly assumed throughout the preceding analysis that the externally applied load is quite steady. Although this is often the intent, it is well recognized in practice that the bearing may be subjected to fluctuations of load, both in magnitude and direction, which may be quite severe. It is a desirable trait of a properly designed hydrostatic bearing that the fluid film can absorb such load fluctuations. Generally speaking, this requires that the film can automatically provide the necessary reactive force due to a counteracting build up of film pressure and at the same time retain its integrity as a full-fluid film. This property of the film is known as stiffness.

Stiffness is defined as $(\delta W/\delta h)$ the partial derivative of the load capacity with respect to the film thickness.

A proper appreciation of bearing stiffness requires consideration of the lubricant flow through the supply system and the bearing. Lubricant is supplied from an external source at a pressure, Ps and is fed to the bearing through a restrictor which offers a resistance, $\bar{R}$ to flow; it enters the bearing at a pressure, Po and the bearing itself presents an internal hydraulic resistance, r, to flow before the lubricant is discharged to atmosphere for recirculation. Since the flow rate is constant throughout the whole system

$$Q = \frac{Po}{r} = \frac{Ps - Po}{\bar{R}} \qquad - (15)$$

where

$$r = \frac{\mu C_r}{h^3} \qquad - (16)$$

Rearranging equation (16)

$$Po = Ps \cdot \left(\frac{r}{\bar{R} + r} \right) \qquad - (16a)$$

Substituting Po in equation (8) to obtain the load capacity

$$W = Ao.Po = Ao.Ps \cdot \left(\frac{r}{\bar{R} + r} \right) \qquad - (17)$$

Differentiating this expression with respect to h gives an expression for the bearing stiffness K.

$$K = \frac{\delta W}{\delta h} = - Ao.Ps \left[\frac{1}{1 + \bar{R}/r} \right]^2 \frac{\delta(\bar{R}/r)}{\delta h} \qquad - (18)$$

Film stiffness can be obtained if the functional dependence of internal and external hydraulic resistance on film thickness is known. As would be expected, and as can easily be shown from equation (18), the film stiffness disappears as the internal resistance becomes very small.

There are three main categories of external resistance:

(1) Laminar restrictors

(2) Fixed orifice restrictors, and

(3) Variable servo-mechanism restrictors.

Laminar restrictors, such as capillaries, are characterized by the fact that the external resistance is independent of both flow rate and film thickness. Therefore:

$$\frac{\delta(\bar{R}/r)}{\delta h} = - \frac{\bar{R}}{r} \cdot \frac{1}{r} \cdot \left(\frac{\delta r}{\delta h} \right) \qquad - (19)$$

$\delta r/\delta h$ is obtained from equation (15). Substituting in equation (19):

$$\frac{\delta(\bar{R}/r)}{\delta h} = \frac{3\bar{R}}{rh}$$

and substituting this in equation (18)

$$K = - \frac{3 \text{ Ao Ps}}{h} \cdot \left(\frac{\bar{R}r}{(\bar{R} + r)^2} \right) \qquad - (20)$$

Fixed orifice restrictors are characterized by the fact that the external resistance is approximately linearly proportional to the flow through the restrictor, and hence indirectly proportional to the film thickness h. Therefore:

$$\frac{\delta(\bar{R}/r)}{\delta h} = - \frac{\bar{R}}{rh} \cdot \left(\frac{\delta r}{\delta h} \right) + \frac{1}{r} \cdot \left(\frac{\delta \bar{R}}{\delta Q} \right) \cdot \left(\frac{\delta Q}{\delta h} \right) \qquad - (21)$$

Using equations (15), (16), (16a) and the equation for resistance of an orifice

$$R = DQ$$

where D is a proportionality constant we get:

$$\frac{\delta(\bar{R}/r)}{\delta h} = \frac{3\bar{R}}{hr} + \frac{3\bar{R}}{hr} = \frac{6\bar{R}}{hr}$$

Therefore the stiffness is

$$K = - \left(\frac{6 \text{ Ao Ps } \bar{R}r}{h(r+\bar{R})^2} \right) \qquad - (22)$$

This relationship is applicable to the present study where a fixed orifice restrictor, a needle valve, was employed.

Servo mechanism restrictors have been discussed in detail by Royle, Howarth and Hayford (6) who have shown that such restrictors can produce infinite stiffness up to the full load capacity of the bearing.

The Effect of Bearing Tolerance on the Pressure Field

Thus far, several important parameters of hydrostatic bearing performance have been considered, based on the assumption that the pressure field is Laplacian. Early in the experimental programme it was found that film pressures measured in the central diametral plane showed surprisingly large peaks which often extend over each of the land areas and deviated considerably from the idealised Laplacian predictions. Since such deviations, if real, affect the values of all parameters examined so far it was decided to investigate their origin.

It was suspected that the pressure peaks might arise from hydrodynamic effects in convergent nips associated with very small bearing tolerances, despite the fact that the design tolerance specifications were felt to be both adequate and realistic. An analysis was therefore made to obtain an order of magnitude of the effect of bearing tolerance on the pressure profile over the land area. This analysis was conducted early in the experimental programme to ensure that there were no serious instrumental faults. Although it does anticipate to some extent experimental data reported later it is presented at this stage for reasons of continuity.

Assuming that the journal rotates about the true centre of the bearing, which is a fictitious position, the variation of radial clearance will be a function of machining tolerances. A nominally round bearing shell can be non-circular and still show fluctuations in diameter within the prescribed tolerances, if such tolerances are obtained solely by measurement of the diameter. However, if the tolerances are measured as radial deviations by a total indicator reading - T.I.R., taken from some

point external to the bearing shell, the deviations may exceed half the specified diametral tolerance as seen in Fig. 10, where the results of a T.I.R. on the test bearing are given. A slight amount of wear was visible in the bearing when these measurements were made. It is seen that variations in radial clearance of the order of 25% were present whereas variations of only 5% were expected according to the design specifications of $0.004 \begin{smallmatrix} + 0.0000 \\ - 0.0002 \end{smallmatrix}$ in. in diametral clearance. In view of this, the applicability of Laplace's equation for the determination of the pressure distribution becomes questionable and Reynold's equation, which allows for variation in radial clearance, must be employed.

Since the pocket depth is fifty times greater than the radial clearance at the lands, normal tolerances will not affect the pressures across the pockets; the land areas are the only regions of concern. Since it would be difficult to describe the variation of radial clearance, h, shown in Fig.10 as a continuous angular function around the circumference, a linear angular variation is assumed over the axial land areas as follows:

$$h = Ho\,(1 + B\theta') \qquad - (23)$$

where

$$\theta' = (2\pi/9 - \theta) \qquad - (24)$$

Ho is the nominal radial clearance. B is a constant and represents the fractional change in radial clearance per degree over a range of 40°, the angle subtended by the centre points of adjacent lands, between which points the T.I. readings were taken. In the present instance B can have values between zero and $(0.25)/2\pi/9$. The convention adopted for the angles allows for the fact that as θ increases in the direction of rotation of the journal, θ' decreases and the nip is convergent as seen in Fig. 11.

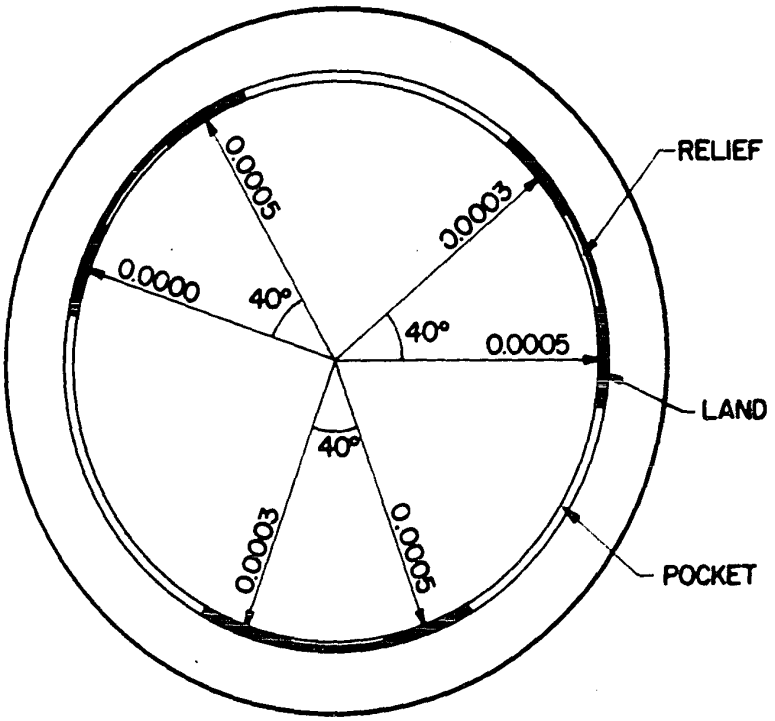

FIG. 10

Total indicator readings over the land areas in the central diametral plane of the test bearing. All dimensions are in inches.

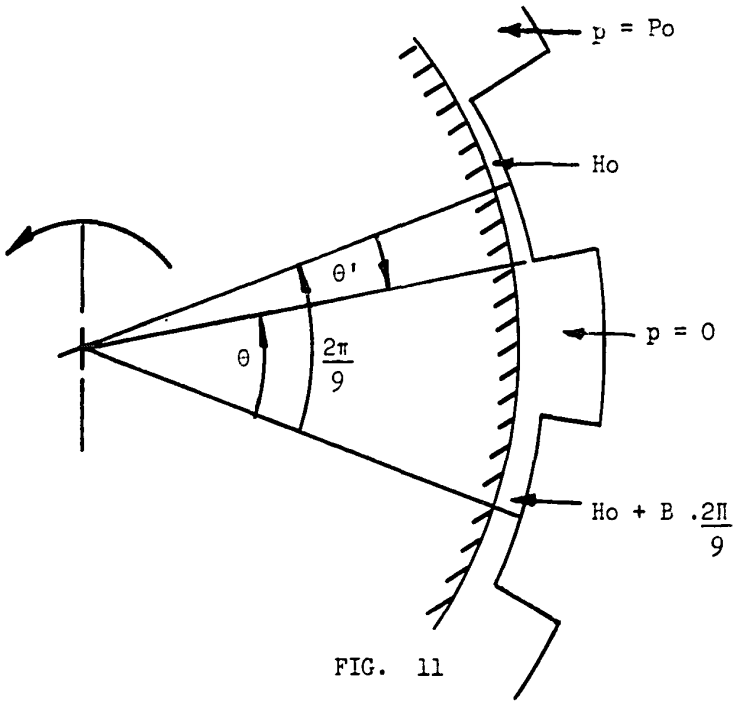

FIG. 11

Since the pressure profiles are considered only in the central diametral plane and there is no pressure gradient normal to this plane, Reynold's equation (3) may be expressed as follows:

$$\frac{\delta}{\delta\theta}\left(h^3 \frac{dp}{d\theta}\right) = 6\,\mu\,U\,R\left(\frac{\delta h}{\delta\theta}\right) \qquad - (25)$$

where $x = R\,\theta$ and R is the radius of curvature of the bearing land. Integrating this equation,

$$h^3 \frac{dp}{d\theta} = 6\,\mu\,U\,R\,h + C \qquad - (26)$$

Since the pressure goes continuously through a maximum value for a convergent nip at some value, h_o, of the radial clearance:

$$\frac{dp}{d\theta} = 0 \text{ when } h = h_o$$

Thus,

$$\frac{dp}{d\theta} = \frac{6\,\mu\,U\,R\,(h - h_o)}{h^3} \qquad - (27)$$

Substituting h from equation (23), and using the relation $d\theta' = - d\theta$ obtained by differentiating equation (24), in equation (27), and integrating, the following expression is obtained for the pressure over the lands:

$$p = - \frac{6 \mu U R}{H_o^3 B} \left[\frac{H_o}{(1 + B\theta')} - \frac{h_o}{2(1 + B\theta')^2} \right] + C_1 \qquad - (28)$$

This expression for the pressure, expressed in terms of the total indicator readings between the centres of adjacent lands can be applied along each of these lands separately assuming that the rate of convergence is constant. A more accurate estimate of the pressure distribution could have been obtained by taking T.I.Rs over each land area.

Using boundary conditions over a single land from the pressure relief at which P = 0 to the pocket where P = Po;

$$p = 0, \ \theta' = \theta_1' = \Pi/9$$

$$p = Po, \ \theta' = \theta_2' = 2\Pi/9$$

values for C_1 and h_o can be found,

$$C_1 = \frac{6 \mu U R}{H_o^3 B} \left[\frac{H_o}{(1 + B\theta_1')} - \frac{h_o}{2(1 + B\theta_1')^2} \right] \qquad - (29)$$

$$h_o = \frac{BH_o^3 Po/6\mu UR - H_o \left[1/(1 + B\theta_2') - 1/(1 + B\theta_1') \right]}{1/2(1 + B\theta_1')^2 - 1/2(1 + B\theta_2')^2} \qquad - (30)$$

Substituting these values of C_1 and h_o into equation (28) yields an expression for the pressure at any point over the land area.

Plots of this function for various values of T.I.R. are given in Fig.12.

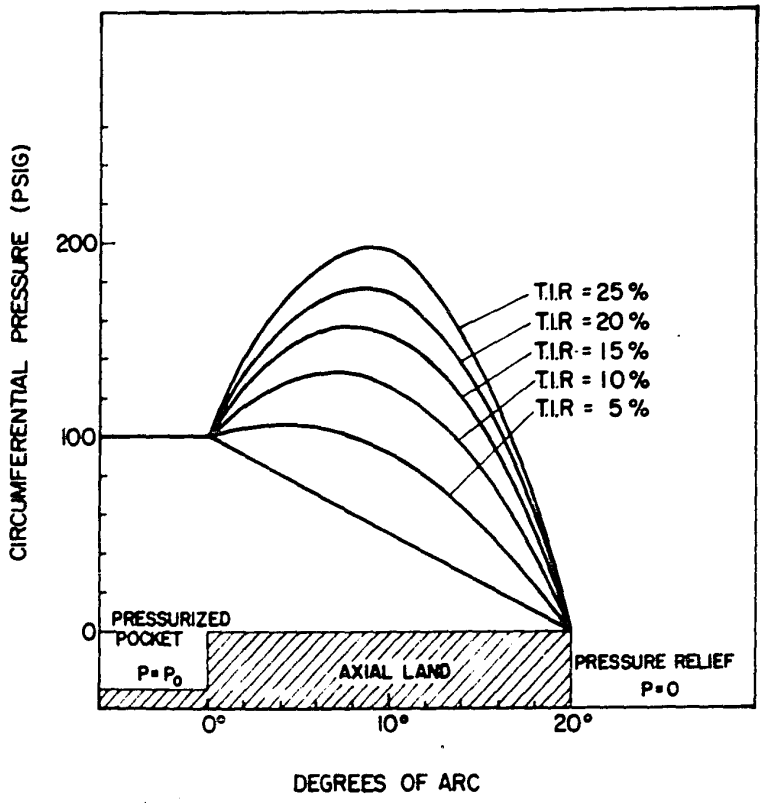

FIG. 12

The distortion of the Laplacian pressure profile over an axial land due to dimensional tolerances in the bearing. The dimensional tolerances are expressed in terms of deviations in the radial dimension along each land from the T.I.R. It is assumed that the gradient of these deviations is linear along the land. The total gradient is expressed as a percentage of the nominal radial clearance and denoted % T.I.R. A significant hydrodynamic pressure component, calculated in the above graph for a journal speed of 1000 r.p.m., is superimposed on the Laplacian pressure profile for even small values of % T.I.R.

Friction Torque

The friction torque of a hydrostatic journal bearing may be broken down into three components; that due to laminar shearing of lubricant under the axial lands, that due to laminar shearing under the circumferential lands and that due to shear in the pressurized pockets.

When a hydrostatic bearing having relatively deep pockets is operated at low speeds the shear stress in the pocket is only a small fraction of the total shear and may be neglected. However, when the bearing is operated at high speeds, as in the present study, a pressure gradient is developed along the pocket due to the step bearing effect (8), giving rise to circulatory flow of lubricant in the pocket. Typical pressure distributions and velocity profiles over various sections of a bearing pad operating under these conditions are shown in Fig. 13.

It will be appreciated from the figure that when the bearing is operated under conditions in which circulatory flow occurs in the pockets, the shear stresses transmitted to the journal from the lubricant film over the pockets and axial lands cannot be calculated independently. Effects occurring in the pockets must be combined with those occurring over the axial lands for the calculation of these stresses. Shear stresses in the lubricant film over the circumferential lands are calculated separately.

Considering first the shear over the axial lands and the pockets in a single bearing pad. Each velocity profile is described by the following general equation, which neglects end effects.

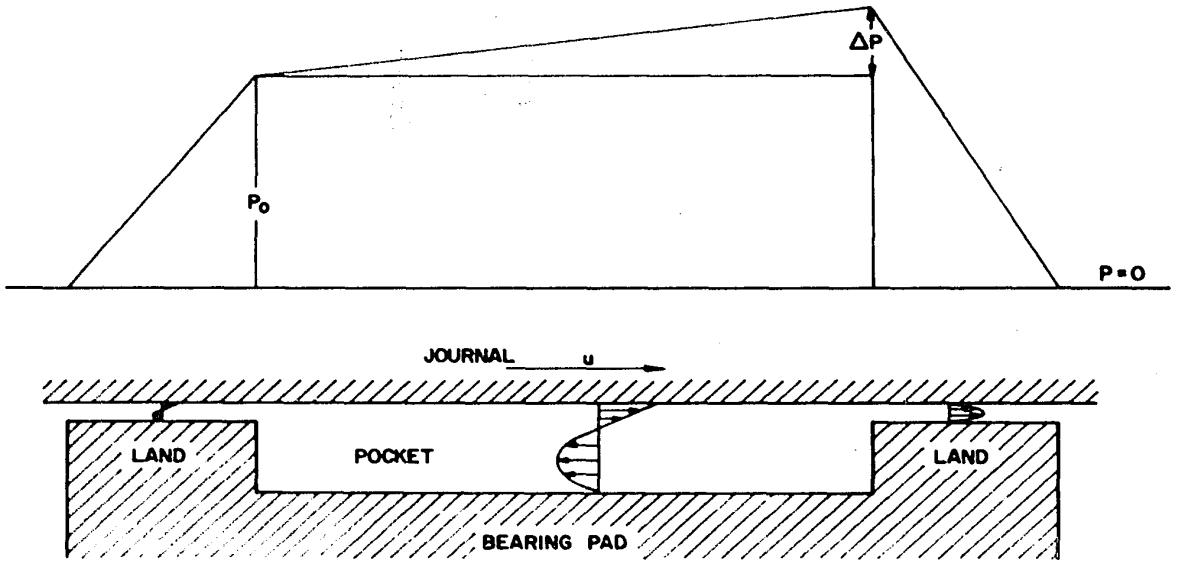

FIG. 13

Lubricant velocity profiles resulting from combined hydrostatic and shear flow over various sections of a developed bearing pad. The resultant distortion, ΔP, of the Laplacian pressure profile due to circulatory flow in the pocket is shown above.

$$u = \frac{y}{h}\left[v - \frac{h}{2\mu}\frac{dp}{dx}\left(h - y\right)\right] \qquad - (31)$$

End effects are neglected since the circumferential flow paths in the pocket and the axial lands are large compared with the respective film thicknesses. Thus, it is assumed that the velocity profiles and the pressure gradients do not change along the length of the bearing pad.

The pressure gradient along the pocket is,

$$\frac{dp}{dx} = \frac{\Delta P}{L_p} \qquad - (32)$$

the pressure gradient along the exit land is,

$$\frac{dp}{dx} = \frac{Po + \Delta P}{L_L} \qquad - (33)$$

and the pressure gradient along the entrance land is,

$$\frac{dp}{dx} = \frac{Po}{L_L} \qquad - (34)$$

Where L_p and L_L are the circumferential lengths of the pocket and axial lands respectively.

It is also assumed that only a small fraction of the lubricant entering the pocket through the feed hole escapes over the circumferential land and that this fraction is negligible compared to the total circulatory flow. This assumption is not justified for very low journal speeds but at higher speeds where the frictional torque is large the assumption is valid. It should also be noted that as the pocket pressure increases, the hydrostatic flow increases relative to the circulatory flow and a greater fraction

of the lubricant escapes over the circumferential land.

In the interests of simplicity the flow will be treated as two dimensional. To satisfy continuity requirements the net outflow from the pocket must equal the net flow through any cross section of the pocket therefore:

$$\underset{\text{pocket}}{\int_0^{h_p} u\,dy} = \underset{\text{entrance land}}{\int_0^{h_L} u\,dy} + \underset{\text{exit land}}{\int_0^{h_L} u\,dy} \qquad - (35)$$

Substituting equations (31), (32), (33) and (34) into (35) and integrating gives,

$$\underset{\text{net pocket flow}}{\left[\frac{Uh_p}{2} - \frac{h_p^3}{12\mu}\frac{\Delta P}{L_p}\right]} = -\underset{\text{entrance land flow}}{\left[\frac{Uh_L}{2} - \frac{h_L^3}{12\mu}\frac{Po}{L_L}\right]} + \underset{\text{exit land flow}}{\left[\frac{Uh_L}{2} + \frac{h_L^3}{12\mu}\frac{Po + \Delta P}{L_L}\right]}$$

Solving for the pressure rise, ΔP, along the pocket.

$$\Delta P = 6\mu \left[\frac{Uh_p - \frac{h_L^3\, Po}{3\mu\, L_L}}{\frac{h_L^3}{L_L} + \frac{h_p^3}{L_p}}\right] \qquad - (36)$$

The pressure term in the numerator can be neglected in comparison with the other terms and rearrangement gives,

$$\Delta P = 6\,\mu\, U\, L_p \frac{Y_i}{h_i^2} \qquad - (37)$$

where $i = (p, L)$,

$$\Psi_p = \frac{1}{\left[\frac{h_L^3}{h_p^3} \cdot \frac{L_p}{L_L} + 1\right]} \quad \text{and} \quad \Psi_L = \frac{L_L}{L_p} \cdot \frac{h_p}{h_L} \cdot \frac{1}{\left[1 + \frac{L_L}{L_p} \cdot \frac{h_p^3}{h_L^3}\right]}$$

The velocity profiles may be expressed as,

$$u_{\text{pocket}} = \frac{Uy}{h_p}\left[1 - \frac{3\Psi_p}{h_p}\left(h_p - y\right)\right]$$

$$u_{\text{entrance land}} = \frac{Uy}{h_L}\left[1 - \frac{h_L}{2\mu}\frac{Po}{L_L}\left(h_L - y\right)\right] \qquad - (38)$$

$$u_{\text{exit land}} = \frac{Uy}{h_L}\left[1 + \frac{h_L}{2\mu} \cdot \frac{Po}{L_L}\left(h_L - y\right) + \frac{3\, h_p\, \Psi_L}{h_L^2}\left(h_L - y\right)\right]$$

The shear stress at the journal surface is given in general by,

$$\tau = \mu \left.\frac{du}{dy}\right|_{y = h} \qquad - (39)$$

and therefore the frictional torque, T_p, expended over the pocket is

$$T_p = \tau_p . A . \frac{D}{2} = \frac{\mu\, Ap\, D\, U}{2\, h_p}\left[1 + 3\,\Psi_p\right] \qquad - (40)$$

Similarly the frictional torque, T_A, expended over the combined axial land area is,

$$T_A = \frac{\mu\, U\, A_L\, D}{2\, h_L}\left[2 - 3\frac{hp}{h_L}\,\Psi_L\right] \qquad - (41)$$

Assuming that the flow of lubricant across the circumferential lands

is laminar the torque, T_c, is given by,

$$T_c = \tau_c . A_c . \frac{D}{2}$$

$$= \mu . \frac{U}{h_L} . A_c . \frac{D}{2} \qquad - (42)$$

The expression for the total torque, T, expended over the bearing pad is

$$T = \frac{\mu U D}{2} \left[\frac{A_p}{h_p} \left(1 + 3 \Psi_p \right) + \frac{A_L}{h_L} \left(2 - \frac{3h_p}{h_L} \right) \Psi_L + \frac{A_c}{h_L} \right] \qquad - (43)$$

The viscosity μ in the above expression is dependent upon both temperature and pressure. Over large ranges of pressure (0-10000 p.s.i.) the viscosity pressure relationship for most lubricating oils may be expressed as:

$$\mu = \mu_o e^{\alpha P} \qquad - (44)$$

where α is a constant peculiar to each lubricant and μ_o is the absolute viscosity at the average film temperature over the relevant part of the bearing pad.

For the bearing under test one pocket is maintained at atmospheric pressure and the other two are maintained at a pocket pressure Po. The expression for torque under these conditions becomes,

$$T = \mu_o \left(1+2e^{\alpha Po} \right) . U . \frac{D}{2} \left[\frac{A_p}{h_p} \left(1+3\Psi_p \right) + \frac{A_L}{h_L} \left(2-\frac{3h_p}{h_L} \right) \Psi_L + \frac{A_c}{h_L} \right] \qquad - (45)$$

Bearing Temperature

The operating temperature of a hydrostatic bearing is of critical importance because of the large temperature dependence of viscosity of most lubricating oils. For instance, the viscosity of normal S.A.E. oils

drops about 50% for a 20°F temperature rise between 80° - 100°F. Thus, the operating temperature of the bearing affects those characteristics of bearing performance which involve lubricant viscosity.

The following analysis is concerned only with temperature changes which occur in the bearing and it is assumed that the temperature of the oil entering the bearing is known.

The temperature change of the oil passing through the bearing depends on four distinct phenomena:-

1. The conversion of pressure energy to heat as lubricant passes from the pocket across the lands to the exit. This is denoted as pad pumping power, H_B, and may be expressed as

$$H_B = Po \cdot Q \qquad - (46)$$

Substituting for Q from equation (12) we have

$$H_B = \frac{Po^2\ h^3}{Cr\ \mu} \qquad - (47)$$

2. Dissipation of the power, H_{SL}, required to overcome viscous drag of lubricant over the axial and circumferential land area. This may be expressed as

$$H_{SL} = \tau .\ U .\ A_L \qquad - (48)$$

$$= \frac{\mu\ U^2 .\ A_L}{h_L} \qquad - (49)$$

where A_L is the total area of the axial and circumferential lands, and h_L is the film thickness over the land area.

3. Dissipation of the power, H_{sp}, required to overcome viscous drag of lubricant in the pockets. This may be expressed as

$$H_{sp} = \frac{\mu U^2 A_p}{h_p} \qquad - (50)$$

where Ap is the total projected area of the pockets and h_p is the film thickness in the pocket area. This contribution is considerably smaller than that due to shear over the land areas and is often neglected.

There is a second contribution to heat production in the pocket which arises from circulatory flow of the lubricant in the pocket. This pumping in the pocket results from the pressure gradient set up in the direction of journal rotation referred to in the previous section. Heat is produced by dissipation of the power, H_{pp}, required for the pumping which may be expressed as

$$H_{pp} = Q_c \Delta P \qquad - (51)$$

where Q_c is the circulatory flow rate obtained by integrating the expression for the velocity profile in the pocket, given in equation (38), and ΔP is the pressure gradient across the pocket which is obtained from equation (36). Since the pressure gradient along the pocket is much smaller than that along the land, and is never greater than 10 p.s.i. in the experimental bearing under the chosen operating conditions, it may be expected at first sight that the contribution of the pocket pumping power would be negligible compared with the pad pumping power. In many cases, however, particularly at high rotational speeds and low pocket pressures, the circulatory flow rate is sufficiently large to more than compensate for the relatively small pressure gradient. For instance, when the bearing is operated at 400 p.s.i. pocket pressure and 1000 r.p.m. the circulatory flow rate is 70 times higher than the flow rate over the lands; when the pocket pressure is reduced to

100 p.s.i. at 1000 r.p.m. this ratio increases to 280. This results in a temperature rise in the pocket which is 2-8 times higher than that resulting from pressure dissipation over the lands.

For the sake of completeness it should also be noted that there is a very small contribution due to dissipation of pressure energy from the pressure gradient in the pocket, acting over the exit axial land. This has been neglected.

4. Heat transfer from the lubricant to the bearing and the journal. This can be appreciable especially if the bearing members contain heat sources and sinks. However, in general it can only be roughly estimated since it is dependent upon many factors such as:

1) bearing member convection film coefficients;

2) heat sources and sinks - their locations and magnitudes;

3) thermal conductivity of bearing members;

4) bearing member masses and geometries;

5) whether or not thermal equilibrium is established;

6) lubricant thermal conductivity, specific heat and flow rate.

No estimate of heat transfer has been made since amongst other things it would involve a numerical analysis of heat generation and transfer in the roller bearing which are both sources and sinks in this assembly. Harris (18) has shown that such an analysis is quite complex even after much simplification. It would also involve evaluating the particular test bed as a heat sink and a further numerical analysis of the temperature distributions in the shaft and bearing. A solution to this problem would involve so many approximations as to severely limit its practical worth. Furthermore, it is probable that only a minor amount of the heat generated in the bearing is lost

through convection since the flow-rate is large enough to provide excellent transport of the most of the heat produced when the bearing has been operated for a time sufficiently long to establish thermal equilibrium. Thus, heat transfer to and from the bearing lubricant has been neglected.

The change in temperature across the bearing is expressed as

$$\Delta\bar{T} = (\bar{T}_E - \bar{T}_I) = \frac{1}{Q\ \rho\ c_p\ J}\left[\frac{P_o^2\ h^3}{C_r\ \mu} + \Delta P.\ Q_c + \frac{A_L\ U^2\ \mu}{h}\right] \quad - (52)$$

where ρ is the lubricant density, C_p is the specific heat of the lubricant, J is the mechanical equivalent of heat, T_E and T_I are the exit and inlet temperatures respectively. Q_c is the circulatory flow rate and Q is the hydrostatic flow rate.

The viscosity μ is expressed as

$$\mu = \mu_o\left[\frac{1 + 2e}{3}^{\alpha\ Po}\right] .$$

where a correction has been made for pressure dependence. μ_o is the viscosity at the average temperature of the lubricant in the region where the heat contribution is being calculated. Therefore, μ_o for the land and pocket regions differ in magnitude.

This form of pressure dependence has been employed instead of the general form, as given in equation (44), since in the test bearing only two pockets are at a pressure Po and the third is at atmospheric pressure.

The solution to equation (52) is an iterative one since temperature is implicitly defined in the viscosity terms on the right hand side.

EXPERIMENTAL APPARATUS

Bearing

The test bearing, shown in part in Fig. 14, is a mild steel annulus 6.20in. I.D., 10.00in. O.D. and 4.0in. wide. Three oil supply holes are drilled axially at 120° intervals on a 4 1/16in. radius into one side of the annulus. They are drilled to half the depth of the bearing and connect with radially drilled oil inlet holes which enter the cavity.

The bearing surface configuration is machined into a 0.100in. thick phosphor-bronze sleeve. Three rectangular pockets symmetrically spaced at 120° to each other are cut through the sleeve; each has a width of 3in. and extends over 60° of arc. Axial grooves are machined to a depth of 0.050in. along the full width of the sleeve and extend over 20° of arc midway between each of the pockets. These grooves provide pressure relief between adjacent bearing pads and allow independent pressure control in each pad. The sleeve is press-fitted into the steel annulus so that an oil inlet is centrally located in each pocket. After assembly, the internal land surface of the bearing is machined to a diameter of $\frac{6.0040}{.0038}$ in.

The test bearing is then pressed into the inner race of an S.K.F. (23052) self aligning spherical-roller bearing and clamped. Fig. 15 shows the resulting bearing assembly mounted in the test rig. This arrangement allows a non axially-biased load to be applied to the test bearing and also permits the measurement of friction torque across the lubricant film.

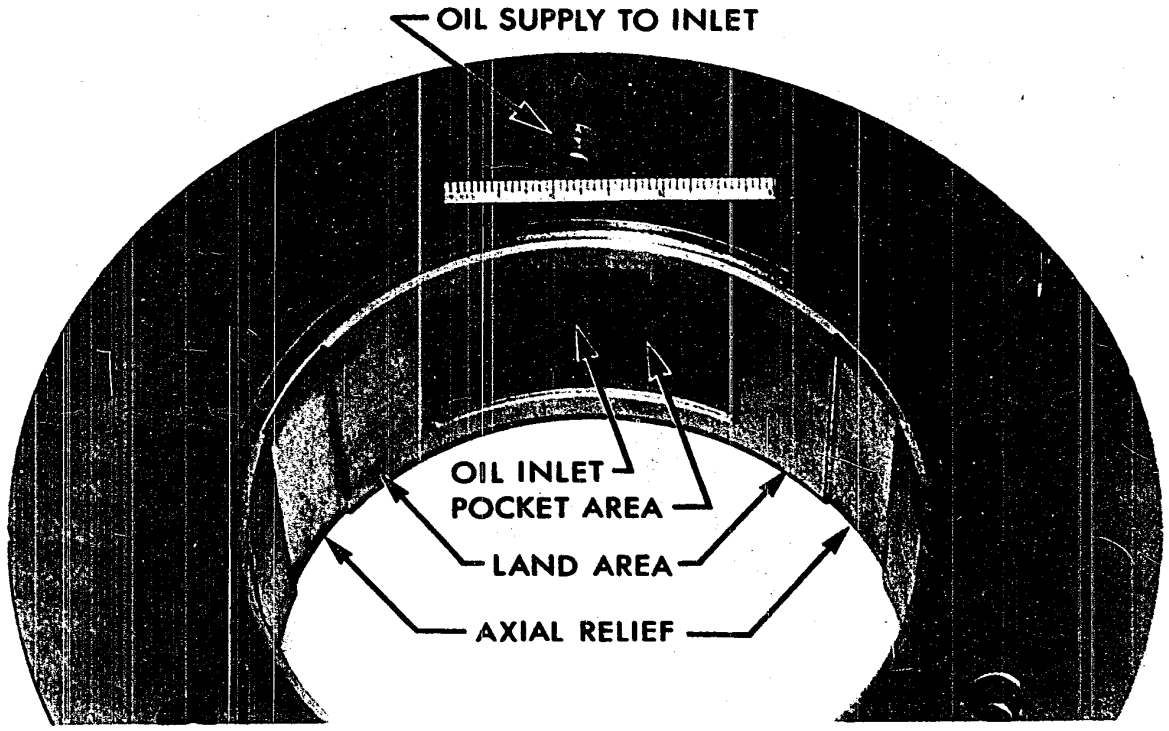

FIG. 14

Hydrostatic test bearing showing one of the bearing pads, the oil inlet to the pocket and the oil supply holes to the bearing.

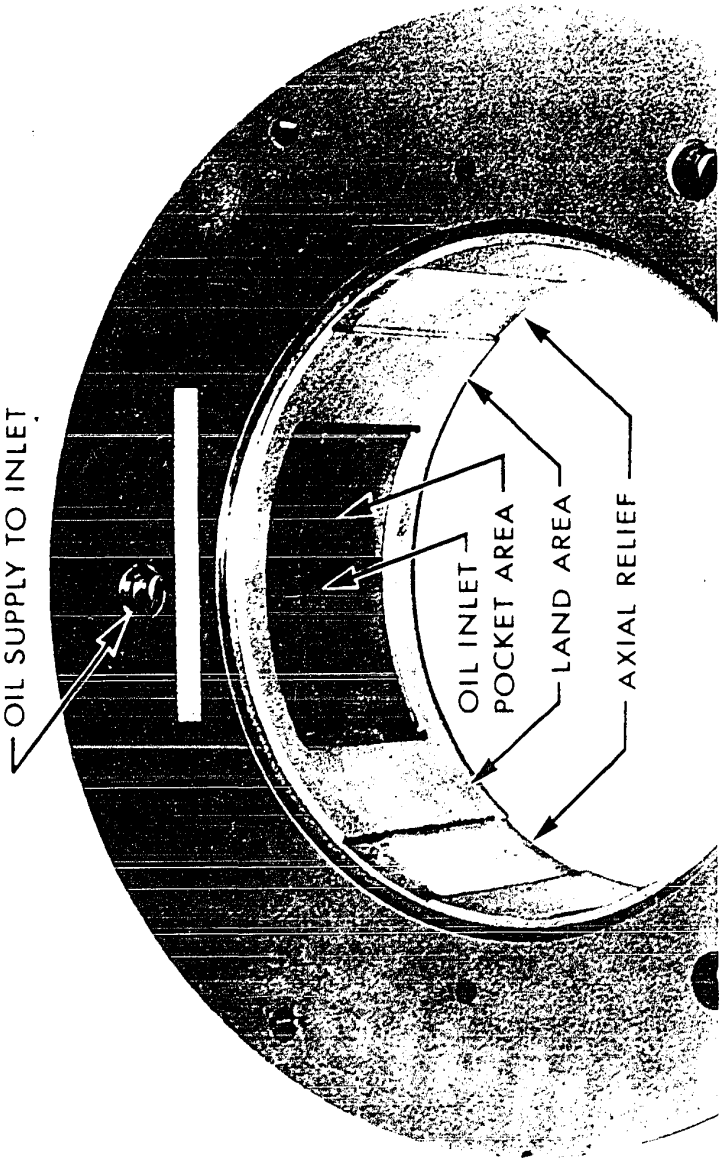

FIG. 14

Hydrostatic test bearing showing one of the bearing pads, the oil inlet to the pocket and the oil supply holes to the bearing.

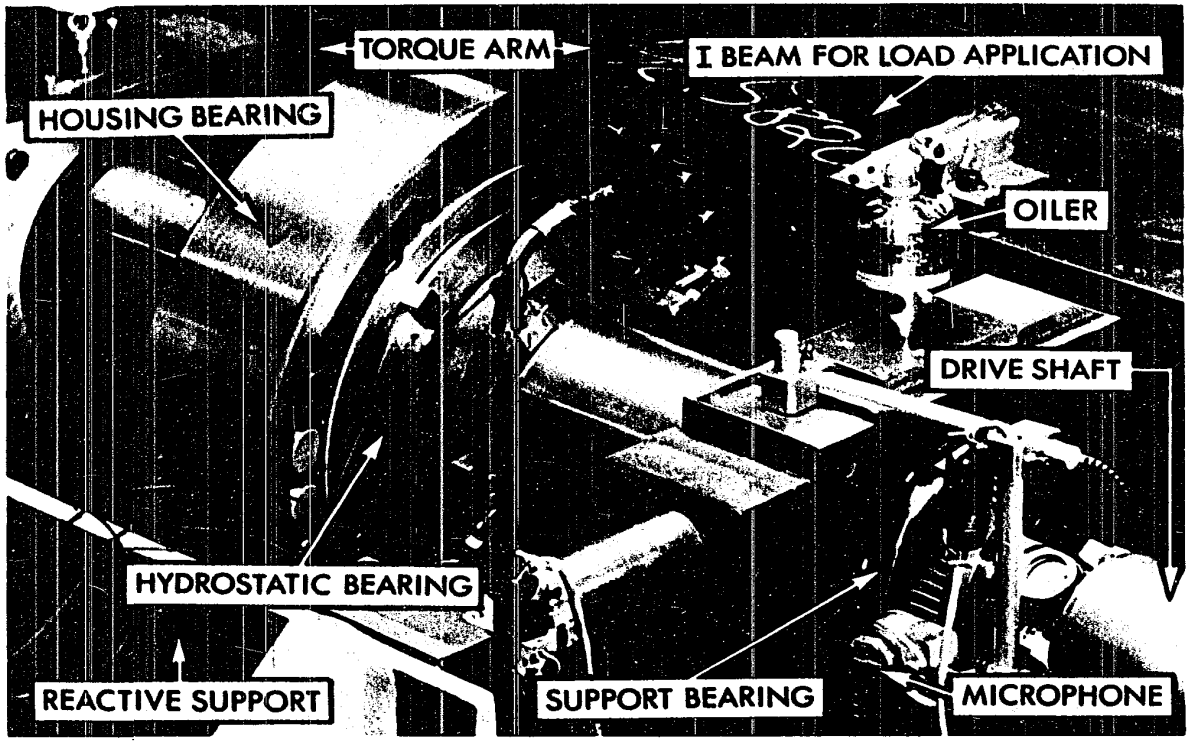

FIG. 15

Bearing assembly in the test rig, showing the journal support bearings and the spherical-roller housing bearing through which the loading force is transmitted to the enclosed hydrostatic bearing. The microphonic, r.p.m. counter is seen to the left of the drive shaft.

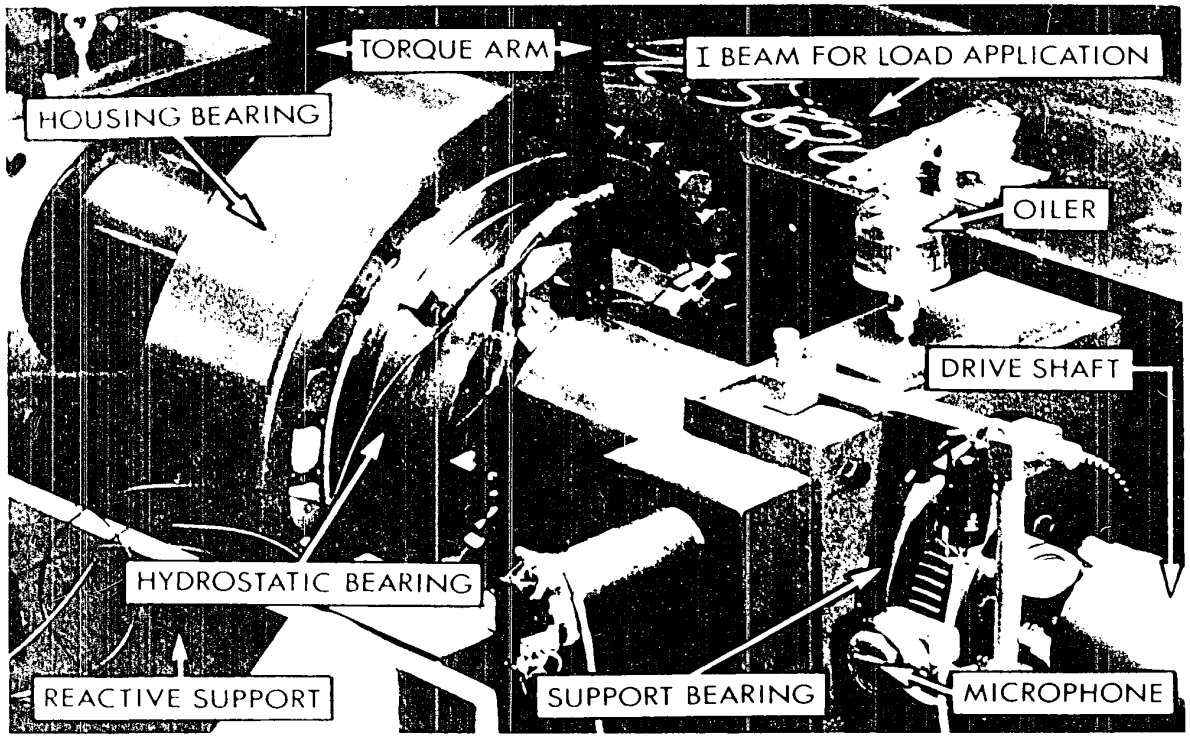

FIG. 15

Bearing assembly in the test rig, showing the journal support bearings and the spherical-roller housing bearing through which the loading force is transmitted to the enclosed hydrostatic bearing. The microphonic, r.p.m. counter is seen to the left of the drive shaft.

Journal

Fig. 16 shows a photograph of the journal. It is machined from 4340 carbon steel to a nominal length of 25in. and a diameter of 6in. and is supported at each end by a Torrington 120 S.D. 23 self aligning spherical roller bearing as seen in Fig. 15. An eight inch width at the centre of the journal is case hardened and ground to a diameter of $6 + \frac{0.0000}{-0.0002}$ in. with a surface finish of 8 microinches. This central part forms the bearing surface of the journal and the radial clearance between the journal and the bearing is 0.002 ± 0.0002in. An annular plug insert, ground to the contour of the journal, is centrally located in the bearing section of the journal to accept a pressure transducer. Electrical leads attached to the transducer are threaded through a 3/8in. diameter hole drilled axially along the centre of the journal from one end and connecting with the radial hole in the insert.

Test Bed

The test bed is a framework of I-beams shown schematically in Fig.17 and in photograph, Fig. 18. A central portion of the flange of each of the longitudinal members is cut away and the resulting web machined to form slide-ways on which the support bearings rest. The framework also provides support for the drive motor and two pneumatic rams which form part of the horizontal loading system. A reinforced angle beam bolted to one end of the longitudinal I-beams provides reactive support for the bearing assembly. Load is applied to the test bearing by the pneumatic rams through a transverse I-beam, which slides along the ways of the longitudinal members to contact the outside race of the test bearing assembly.

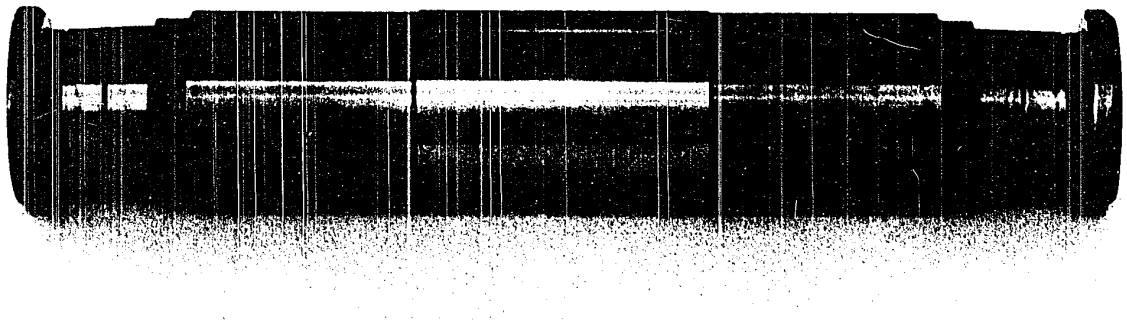

FIG. 16

Photograph of the journal showing the support bearing seats, the test bearing surface and the central hole in this surface in which the pressure transducer is mounted.

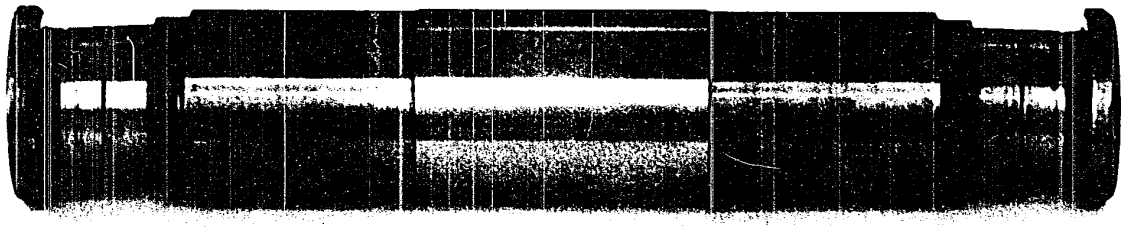

FIG. 16

Photograph of the journal showing the support bearing seats, the test bearing surface and the central hole in this surface in which the pressure transducer is mounted.

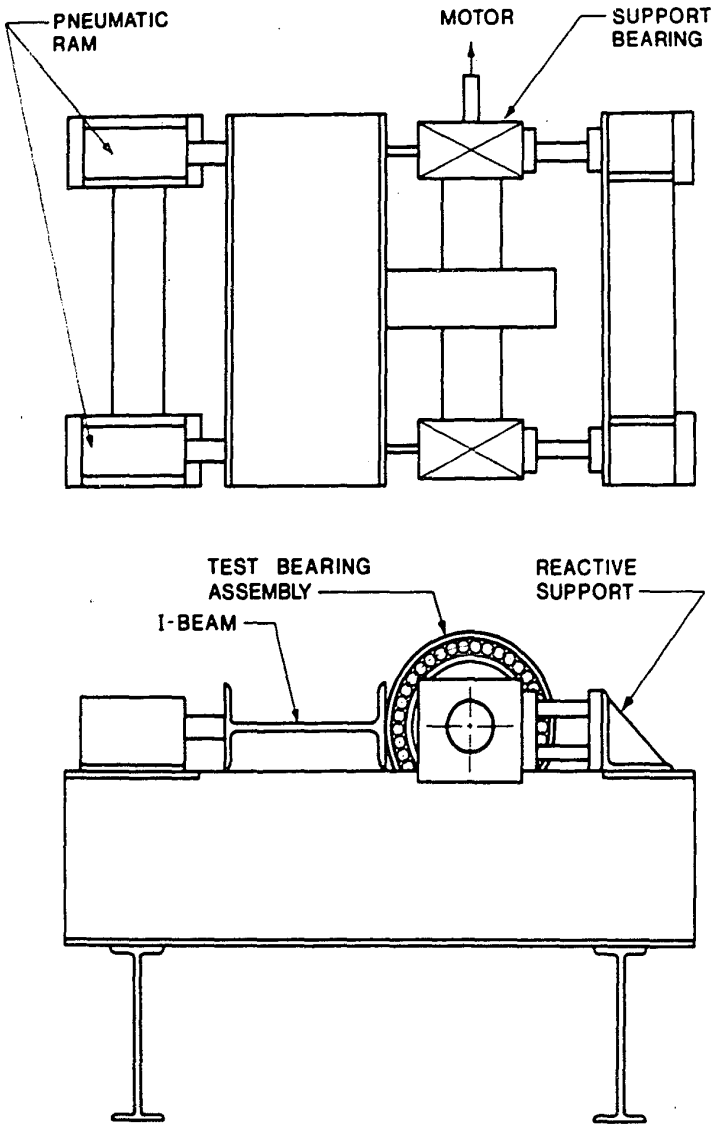

FIG. 17

Schematic showing plan and elevation views of the bearing assembly. The support system and method of load application to the test bearing are illustrated.

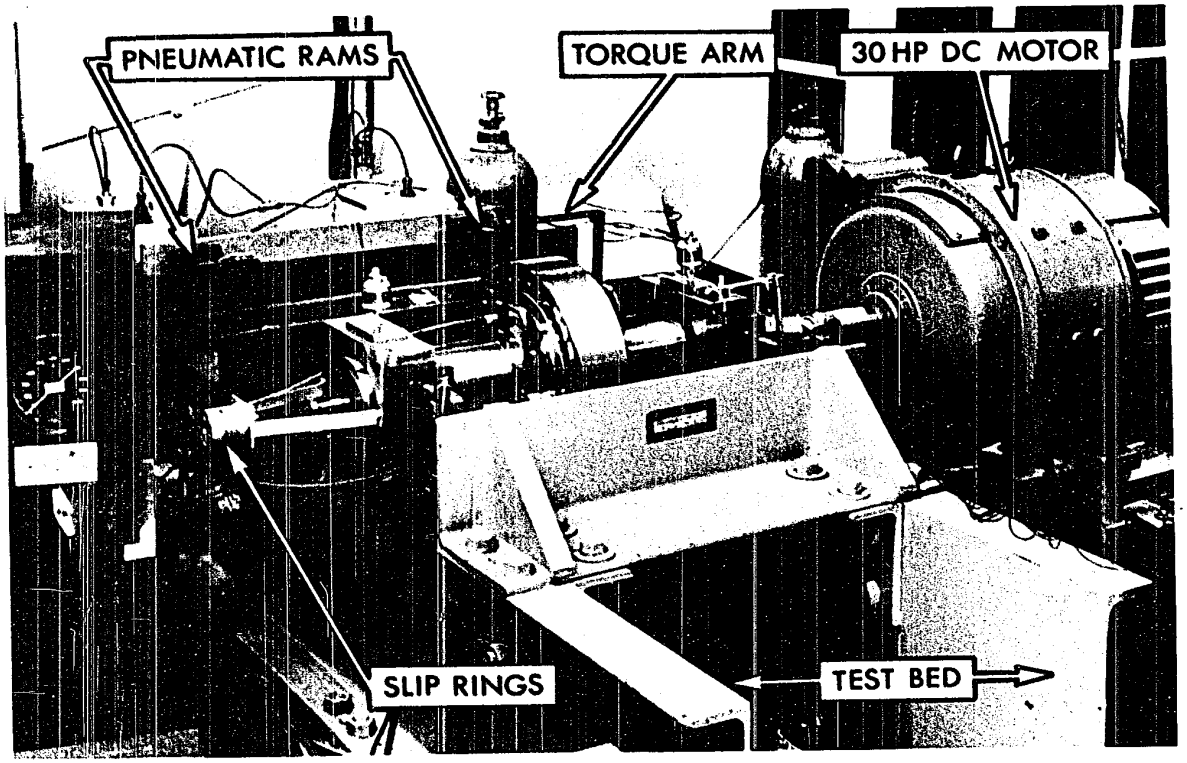

FIG. 18

Photograph showing bearing assembly on test bed, method of load application to test bearing and journal drive.

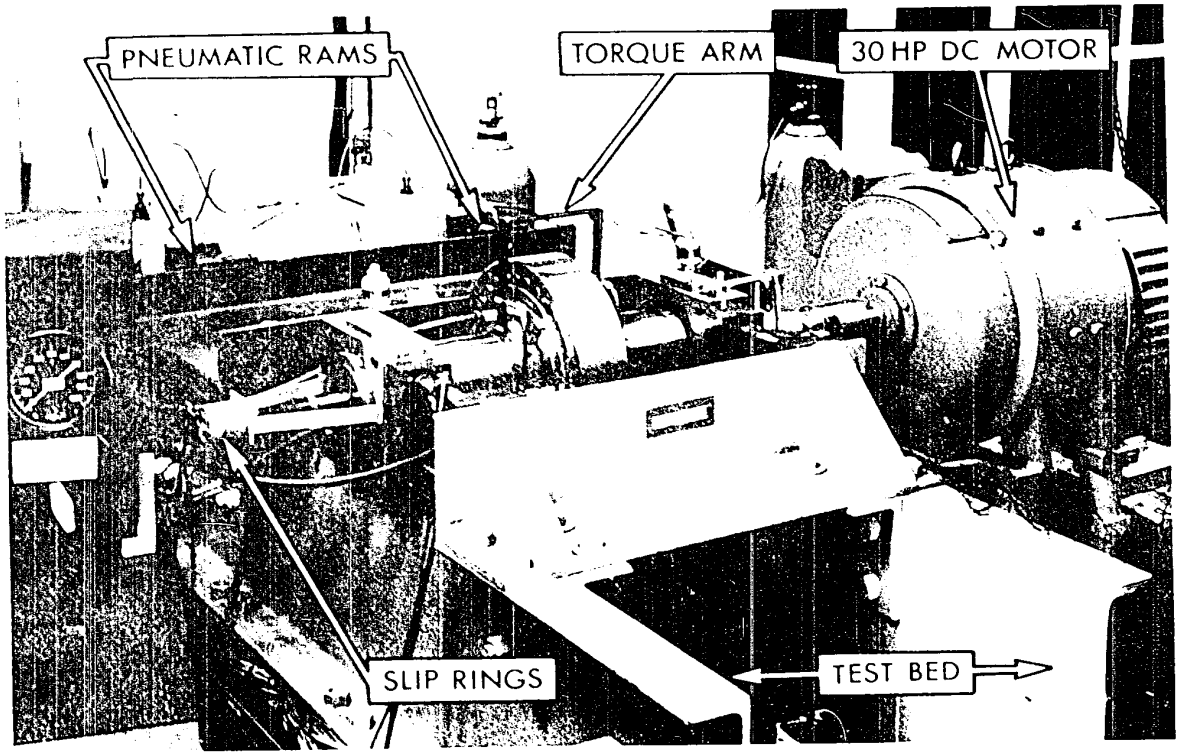

FIG. 18

Photograph showing bearing assembly on test bed, method of load application to test bearing and journal drive.

Load System

The loading system, shown schematically in Fig. 19, consists of two alternate sources of air pressure, a compressor or a compressed air bottle, two pneumatic rams each with a 6in. diameter piston and a pressure balancing system to ensure equivalent loading by each ram. Pressure to each ram is monitored roughly by a 0-1000 p.s.i.g gauge. A master gauge with a range 0-750 p.s.i.g, an accuracy of better than 0.1 per cent of full scale and a resolution of 0.5 p.s.i. is used for accurate pressure measurement. The system can deliver loads through the range 0-42,000 lb. It was built previously for another application and was more than adequate for use in this study.

Drive System

The drive system consists of a 30 H.P. continuously variable speed D.C. motor coupled to a Ward-Leonard speed control system. The journal is driven through a universal joint assembly connected by a floating sheave keyed to the motor shaft. Rotational speeds through the range 50-1200 r.p.m. and controllable to ± 0.075 R.P.M. can be obtained.

Hydraulic System

A type P/N TE-7001 Pacific Air Motive Corporation fluid static test machine was modified for use as a hydraulic supply system to the test bearing. It consists basically of a five gallon reservoir, a vane-type hydraulic pump driven by a 3 H.P. 1200 R.P.M. motor, a micronic filter unit, a heat exchanger, temperature and pressure gauges. The unit is rated to deliver 3 g.p.m. at 700 p.s.i.g, thus allowing an external load

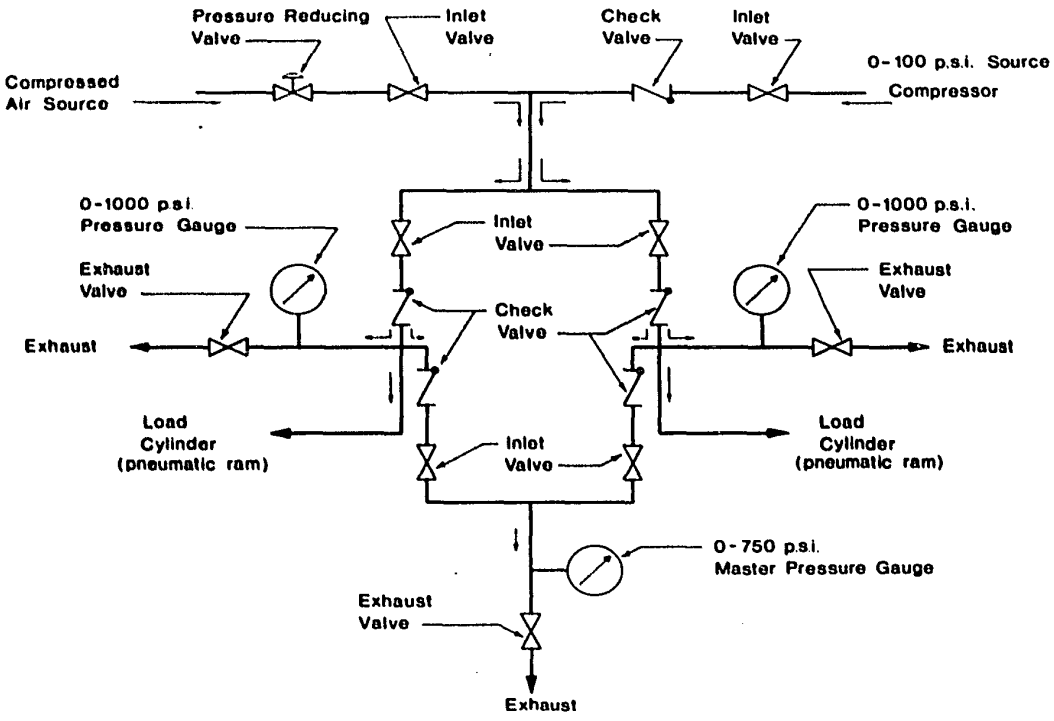

FIG. 19

Flow diagram of pneumatic loading system showing control valves and gauges.

application through the range 0-8000 lb. Due to overheating the maximum practical working pressure was limited to 500 p.s.i.g and the external load application to a range of 0-4000 lb.

Hydraulic pump pulsations are damped by connecting a Hale five gallon capacity nitrogen-oil accumulator in the delivery line. S.A.E. 30 oil is pumped through the accumulator to a four-way manifold where it splits into three lines, one for each bearing pocket. A needle valve restrictor and a 0-1000 p.s.i.g pressure gauge is incorporated into each line and the oil flows to the bearing annulus through flexible pressure hoses. After the oil emerges from the bearing it is trapped in a non-contact thread flinger type seal, shown in Fig. 20, from which it flows to the rate measuring equipment.

Flow rate is measured by catching the oil emerging from the bearing in a catch pan on a weigh scale. When a given weight of oil has flowed into the catch pan a pump motor is activated and the oil is pumped back to the hydraulic unit. The system is calibrated so that a knowledge of the off-on time interval between pumping gives a direct measure of the flow rate.

INSTRUMENTATION

Oil Film Pressure Measurement

The oil film pressure in the central diametral plane of the bearing is measured by a Kistler, type 203A, piezoelectric pressure transducer with a built in charge amplifier as shown in Fig. 21. This is a relatively new type of piezoelectric transducer containing a miniaturized amplifier which allows the signal to be taken through slip rings without being masked by noise.

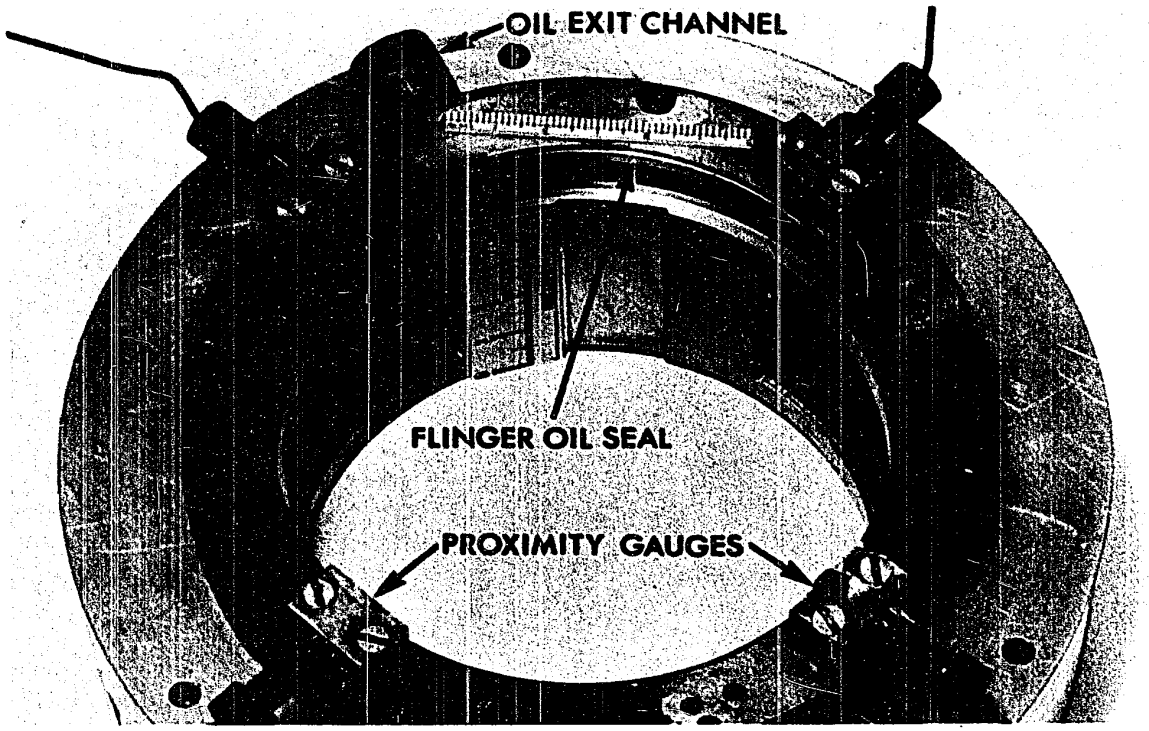

FIG. 20

Hydrostatic test bearing showing mounting configuration of proximity gauges, oil flinger seal and lubricant exit.

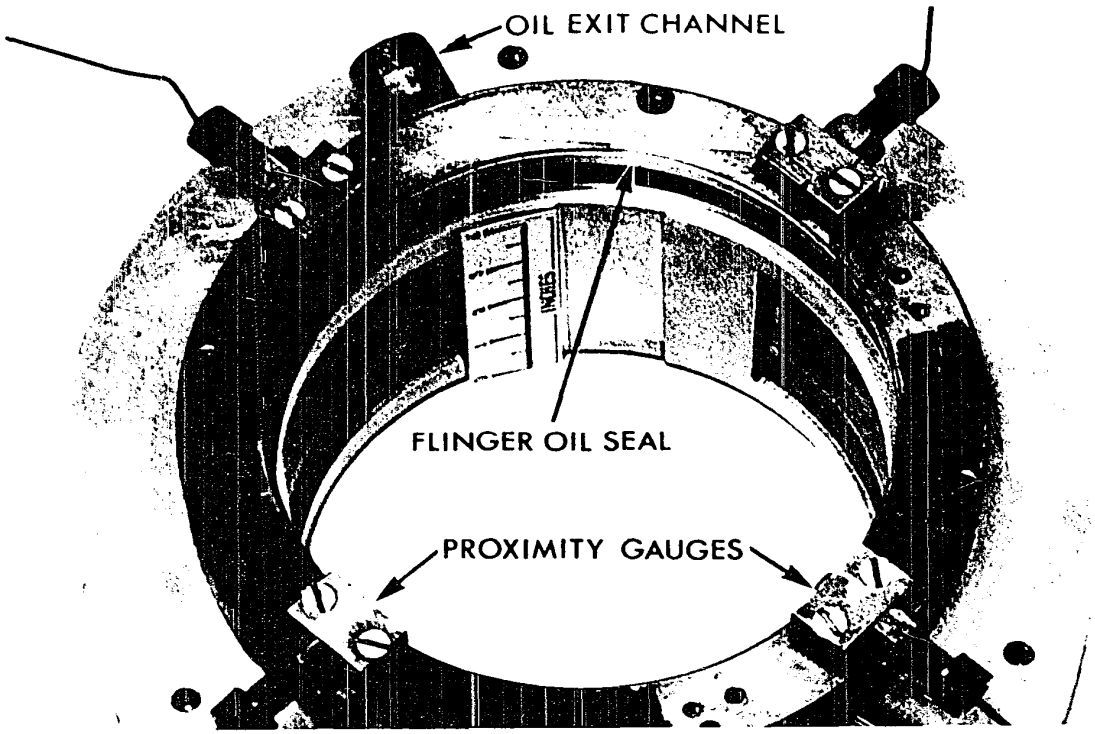

FIG. 20

Hydrostatic test bearing showing mounting configuration of proximity gauges, oil flinger seal and lubricant exit.

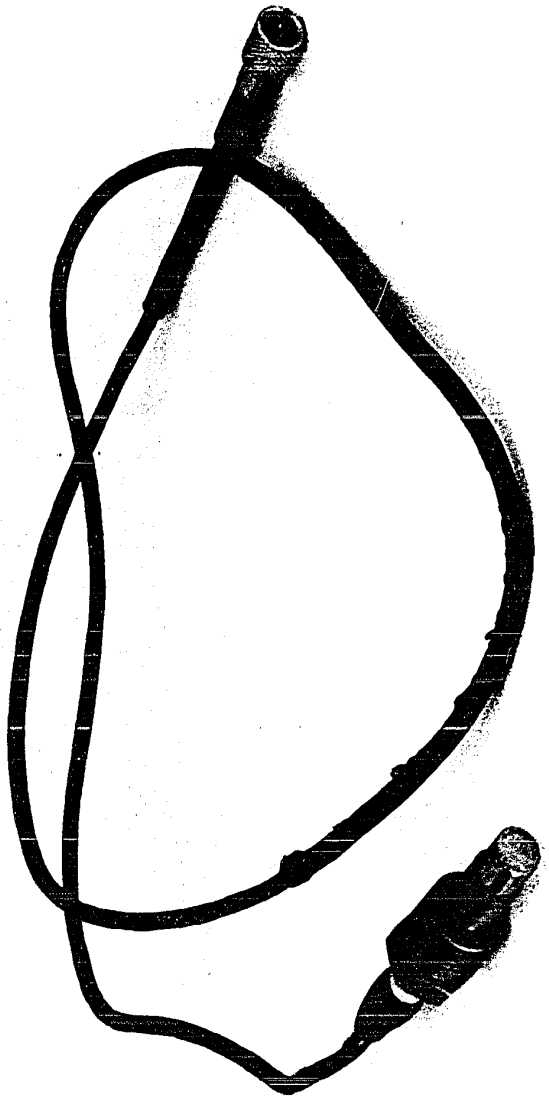

FIG. 21

Piezotron pressure transducer and cable.

The transducer is screwed into the removable insert in the journal so that the plane of the sensing face is between 0.000-0.001in. below the surface of the journal. Attempts were made to apply a thin coat of epoxy cement on to the exposed head of the transducer and contour the resulting surface with that of the adjacent surface of the journal. However, owing to poor bonding between the cement and the transducer head this idea was abandoned.

The charge amplifier is powered by a D.C. battery-coupler which sits on an axially mounted holder at the end of the journal. The circuit diagram of the system is shown in Fig. 22. Pressure induced signals proceed via coaxial cable through M.P.L. type 900 150/1 slip rings and are displayed on a storage type oscilloscope where they are photographed.

The pressure transducer has a full-scale range of 0-1000 p.s.i.g. and a sensitivity of 1.07 mv./p.s.i. It is linear to within 1 per cent of full-scale reading and has a rise time (0-90% full-scale) of one microsecond, hence it is easily able to follow the pressure profile quite faithfully over the speed range employed.

Journal Location

Inductive type proximity gauges, manufactured by Mechanical Technology Inc., are used to monitor the displacement of the centre of the shaft relative to that of the bearing. Since the gauges are temperature sensitive and are mounted on the radial face of the bearing housing which heats up during operation two pairs of active gauges are used to provide for temperature compensation. The gauges in each pair are carefully matched and are located in diametrically opposite positions on each side of the journal. Each pair of gauges form opposite arms of

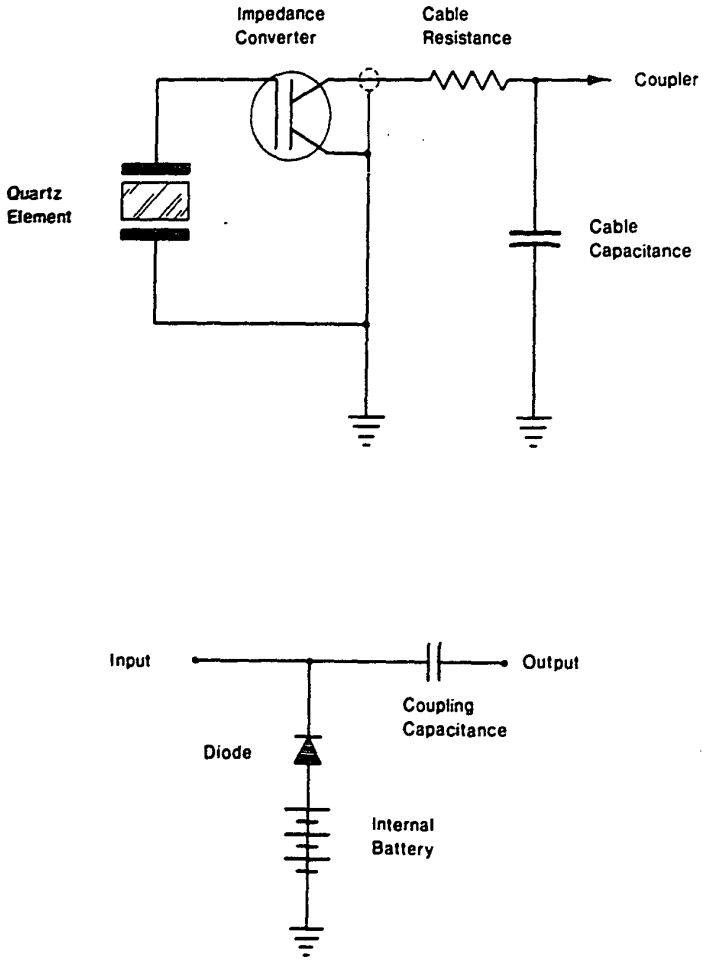

FIG. 22

Circuit diagram for Piezotron transducer and associated charge amplifier.

two separate A.C. bridge networks and fixed inductances, of approximately the same value as the inductance of the probe, are inserted in the other two arms of each bridge. Both bridges are energized by a common 25 k.c. oscillator.

Each gauge is mounted in an Allen screw through which a longitudinal hole is drilled to accommodate electrical leads. The screws are threaded into steel blocks mounted at 90° intervals on the bearing flinger ring as shown in Fig. 20, and the active face of each gauge can be offset a desired distance from the journal surface and held in position by a lock nut.

Both bridges are balanced when the centre of the journal coincides with the centre of the bearing. Any displacement of the journal from this position gives rise to an out of balance condition in one or both of the bridges. These output signals are demodulated, and the resulting D.C. signals from both bridges are fed to the X and Y plates of an oscilloscope. In this manner the position of the journal is constantly monitored and the measurements are independent of the bearing temperature provided there is no appreciable circumferential temperature gradient around the bearing.

Fig. 23 shows a typical calibration curve of an inductive gauge. It is seen that the sensible range extends 0.030in., but that the response is non-linear through the range 0.0075-0.030in. The gauges are offset 0.002in. from the journal surface at the position of closest approach and operate in the linear range 0.002-0.006in. Under these conditions the system is capable of detecting a journal movement of 25 microinches.

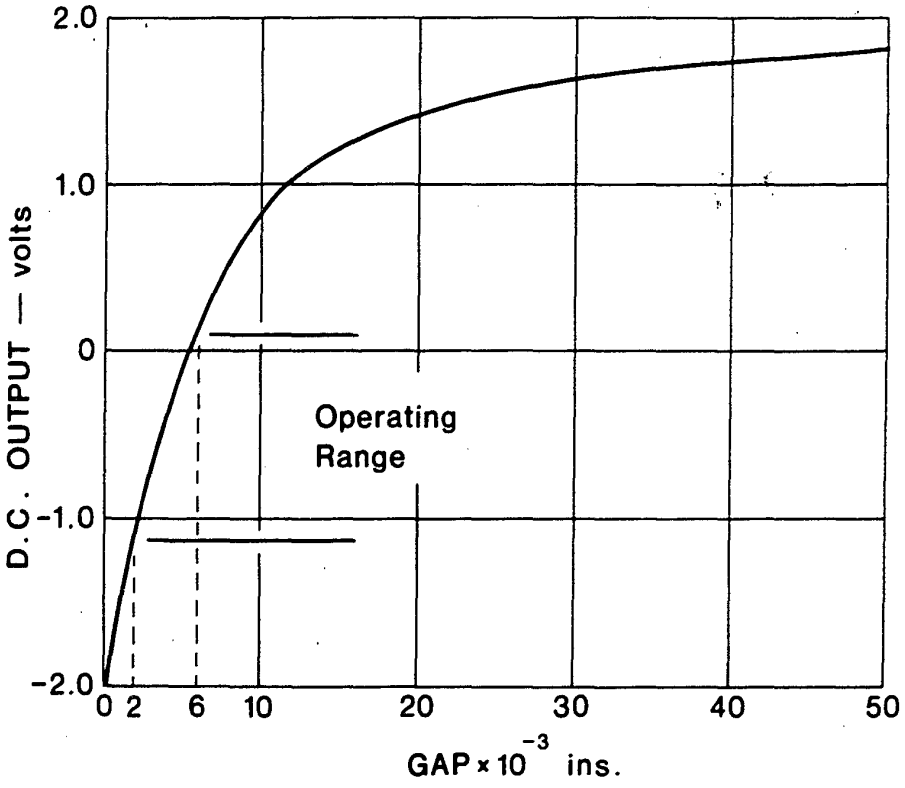

FIG. 23

Calibration curve of output vs.
gap or stand-off distance for
inductive proximity gauges.

Oil Temperature and Angular Velocity of the Journal

Oil temperature is measured by iron-constantan thermocouples, one inserted in the oil inlet supply line and two others inserted inside the flinger seal at the oil exit channel to measure the temperature of the oil leaving the bearing. Thermocouple signals are fed into a Hewlett-Packard Dymec 2010B data acquisition system and printed out at short prescribed intervals.

Rotational speed is measured by a magnet and coil assembly sensing the passage of individual teeth on a gear attached to the drive shaft. As each gear tooth passes the sensor the magnetic field is disturbed and a voltage signal is produced; this signal is fed into the Dymec and printed out.

Fig. 24 is a photograph of the complete test system.

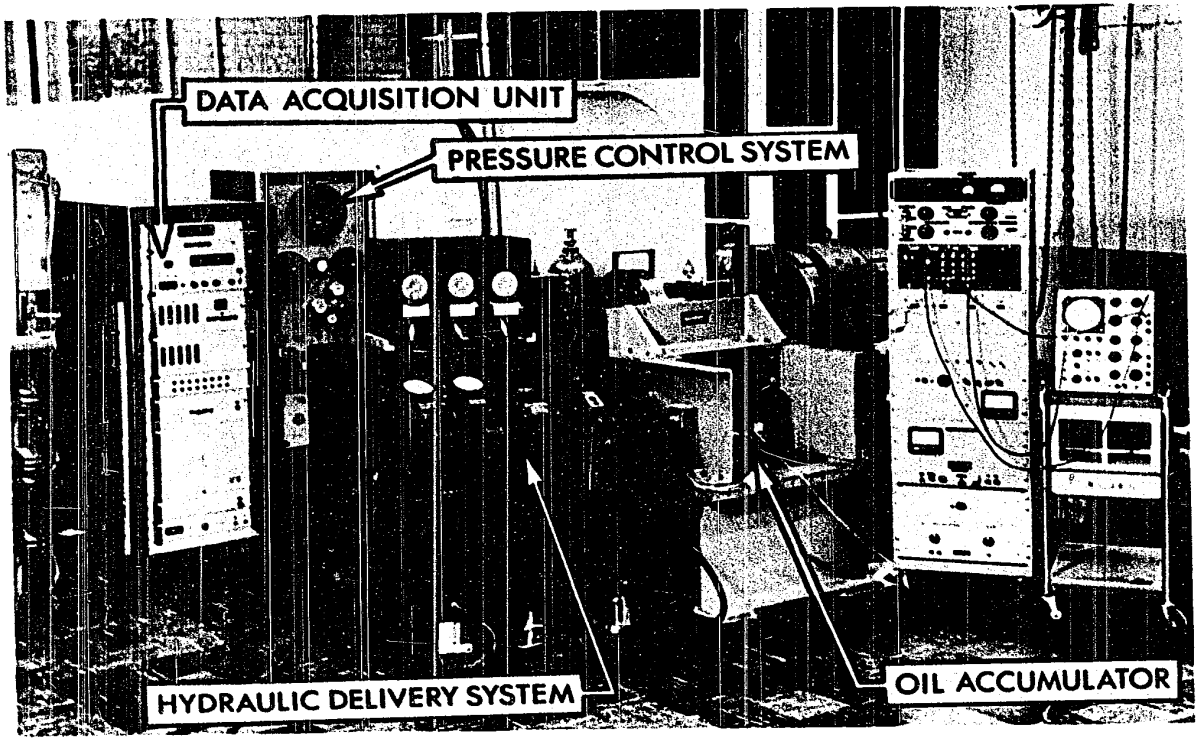

FIG. 24

Complete test facility, showing the hydraulic delivery system, the load control system and the amplifiers and oscilloscope for monitoring bearing eccentricity.

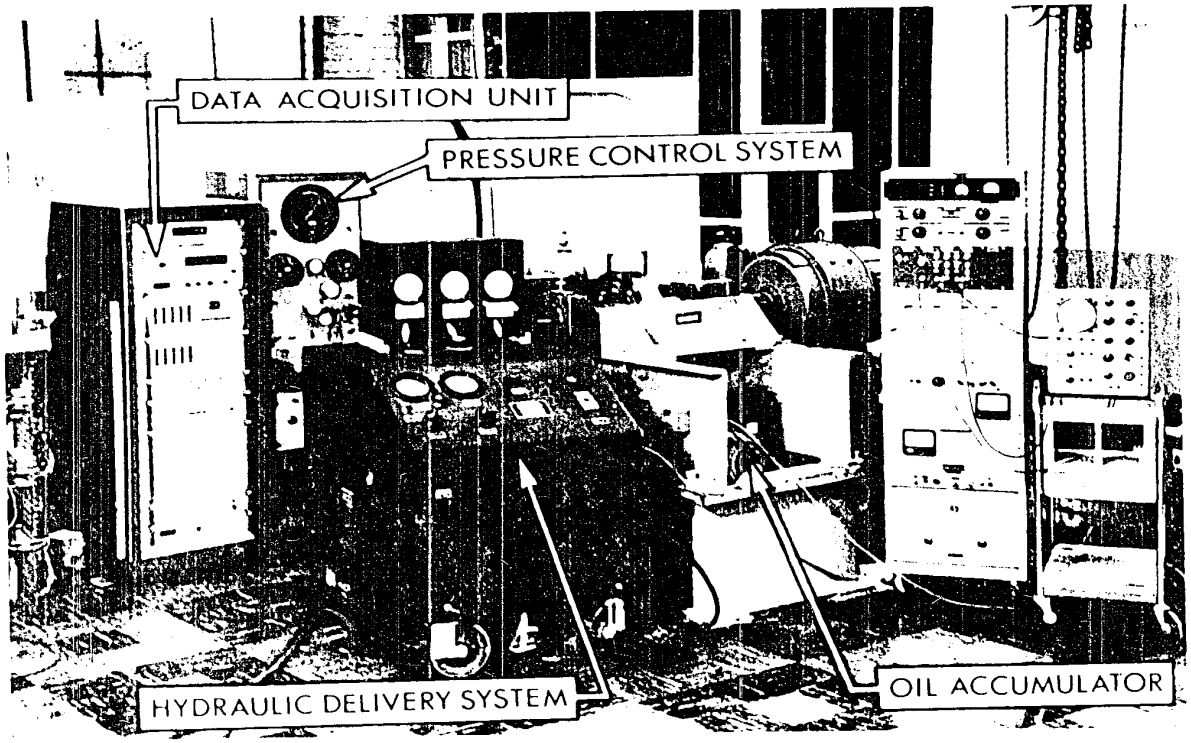

FIG. 24

Complete test facility, showing the hydraulic delivery system, the load control system and the amplifiers and oscilloscope for monitoring bearing eccentricity.

EXPERIMENTAL PROCEDURE

The main part of the experimental program consisted of making measurements of friction torque, the circumferential pressure profile in the central diametral plane, the temperature of the lubricant entering and leaving the bearing, the journal speed and the lubricant flow-rate at loads of 1000, 2000, 3000 and 4000 lb. respectively. At each test load, runs were conducted at journal speeds through the range 100-1000 r.p.m. in steps of 100 r.p.m., maintaining the journal in a position of zero eccentricity. The bearing temperature was allowed to equilibrate before taking any measurements and the bearing temperature did not change more than 1°F during any set of measurements.

A small number of experiments was conducted at a later stage employing non-zero values of the eccentricity.

It was necessary to calibrate the proximity gauges prior to each series of runs at any particular loading. Oil was supplied to each of the three bearing pads at a pressure previously determined to support the relevant test load. The journal was then rotated at 1000 r.p.m., with no external loading, for a sufficiently long time to allow temperature equilibration, so that the proximity gauges attained the operating temperature of the bearing and any drift of gauge output due to temperature change was minimized. The external loading was simulated by applying pressure to pocket 2.

The journal was then stopped and oil pressure was released from the pockets prior to calibration of the gauges. The bearing was

rotated until one pair of gauges lay along a vertical axis. Using a screw jack the bearing was moved in a vertical direction through the range of the film clearance gap and the centre of the range of the gauge output was centered on the oscilloscope. This operation was repeated several times before making the final adjustment on the scope. The bearing was then rotated through 90° so that the other pair of gauges lay along the vertical axis, the procedure was repeated, and the range of the gauge output was again centered on the scope. From an X-Y plot of the outputs from the two pairs of gauges the centre of the bearing can be located.

The test load was then applied and balanced by adjusting the oil pressure to bearing pads 1 and 3, as shown in Fig. 25, to centre the journal. The journal speed was adjusted to 1000 r.p.m. and the lubricant temperature, as measured by the exhaust temperature, allowed to equilibrate. A set of measurements was then made. The journal speed was reduced in steps of 100 r.p.m., to a final setting of 100 r.p.m., measurements being made at each speed setting.

The load was then increased in steps of 1000 lb. to 4000 lb. and the procedure repeated at each loading after calibration of the proximity gauges at the start of each new load test.

The friction shear is measured by resisting the torque on the test bearing with a spring balance. As mentioned previously the test bearing is fixed to the inner race of a spherical roller bearing which allows the test bearing to rotate and torque to be measured. The roller bearing has associated with it a certain amount of starting friction which acts to oppose the rotation of the test bearing and therefore the spring

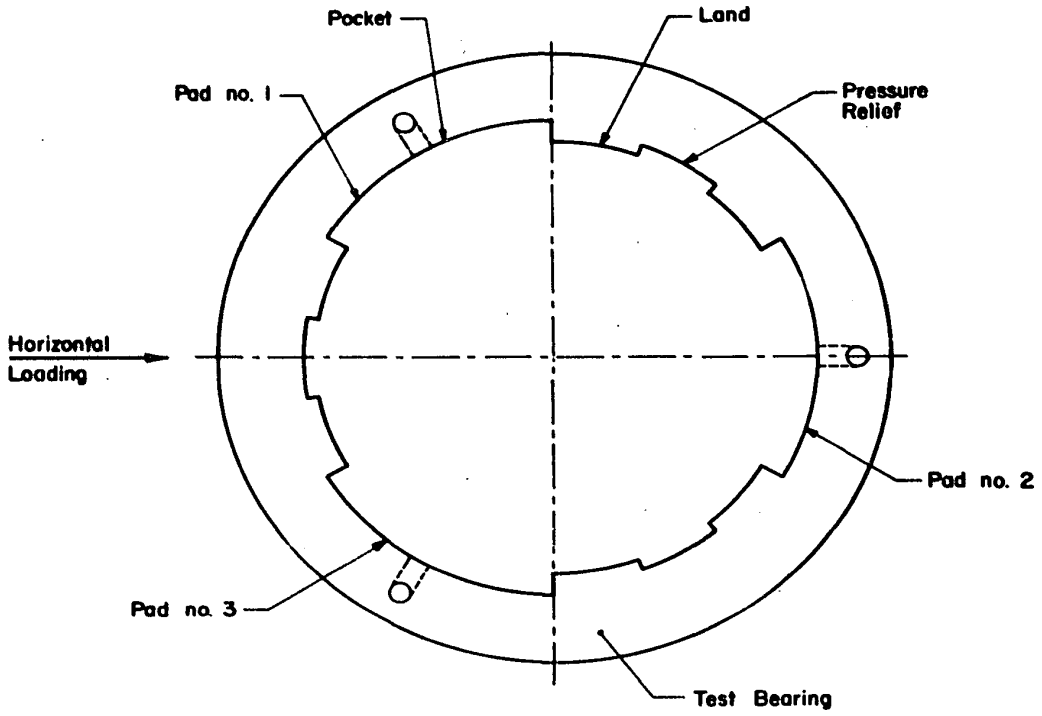

FIG. 25

Schematic of hydrostatic test bearing showing the various parts of the bearing including the lubricant inlet holes and the direction of load application relative to the designated pockets.

balance measures a net torque which is made up of contributions from both the test bearing and the roller bearing. In order to eliminate the starting friction component the torque is measured twice, once allowing the bearing to rotate slowly in the direction of journal rotation, and secondly in a direction opposing journal rotation. Upon adding these two results and dividing by 2 we obtain a value of frictional torque for the test bearing alone. The method is illustrated schematically in Fig. 26.

A series of experiments was conducted to measure the temperature change of the lubricant as it passed through the bearing with no external load, but with the oil pressure in all three pockets adjusted to values of 150, 280 and 400 p.s.i.g. These pressures almost cover the range of load bearing capacity used in the previous experiments.

The three pockets were fed with pressurized lubricant and the pressures were adjusted to centre the journal. The journal was rotated at constant r.p.m. until thermally steady state conditions were set up as indicated by a constant temperature differential across the bearing. Measurements of inlet and outlet temperatures were made at four journal speeds for each pressure.

The results were used to evaluate the theoretical prediction of temperature change of the lubricant in the bearing.

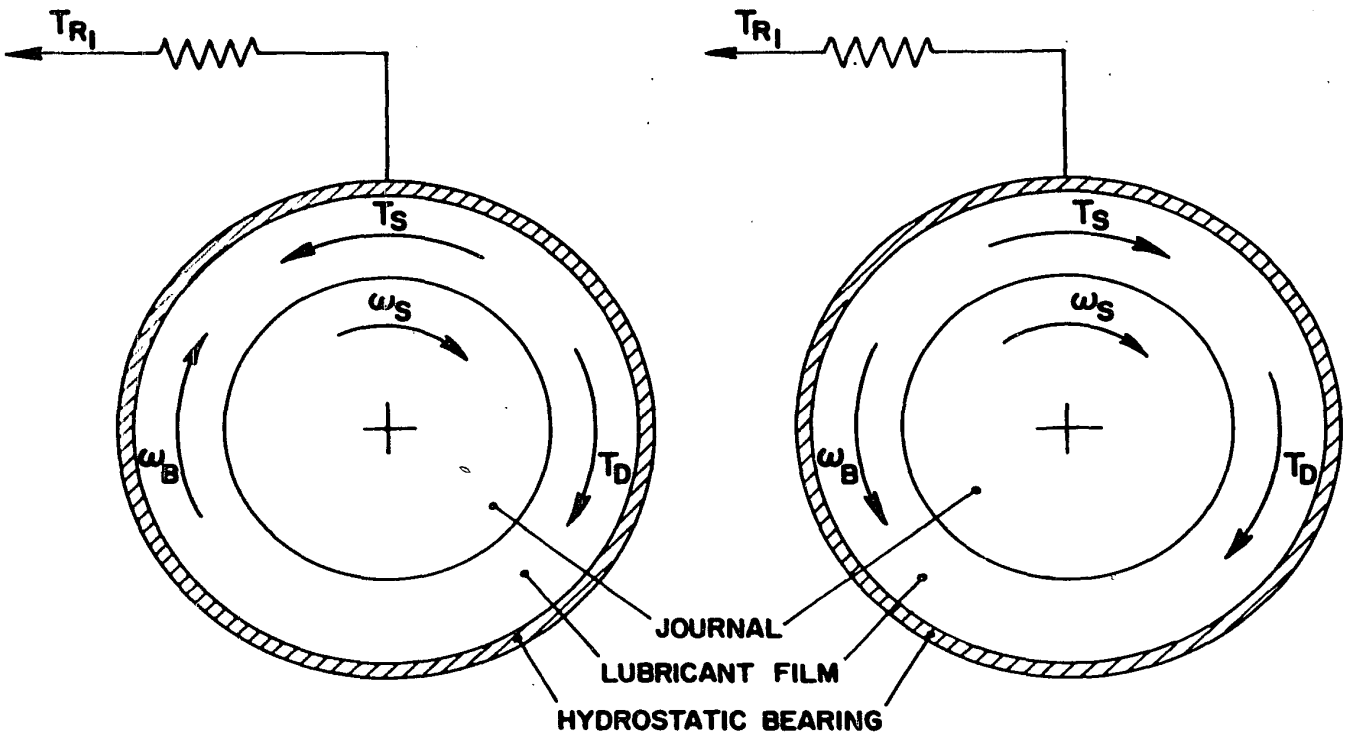

FIG. 26

Schematic showing principle of method for measuring friction torque of hydrostatic bearing. ω_S - direction of shaft rotation, ω_B - direction of bearing rotation, T_R - resisting torque produced by spring balance, T_s - torque due to starting friction opposing ω_B, T_D - torque due to shear in film in direction of ω_S.

$$T_{R_1} = T_D - T_s \qquad T_{R_2} = T_D + T_s$$

$$T_D = \frac{T_{R_1} + T_{R_2}}{2}$$

RESULTS AND DISCUSSION

Circumferential Pressure Profiles

Typical examples of pressure profiles measured in the central diametral plane of the bearing, at various load-speed combinations over a load range of 1000-4000 lb. and a speed range of 200-1000 r.p.m., and photographed on a storage-type oscilloscope are given in Figs. 27-30. Each profile may be matched to the developed bearing configuration by reference to the fact that in all experiments no lubricant was fed to pocket 2, whereas pockets 1 and 3 were always pressurized as shown in Fig. 25.

Inspection of these pressure profiles shows that they differ quite markedly from the shape of the corresponding theoretical Laplacian profiles. Possible reasons for these differences may arise as a consequence of the three following phenomena which were not considered in the derivation of the Laplacian profile:

1. The bearing has a certain diametral machining tolerance. In the bearing under study, assuming the journal to be perfectly round and concentric with respect to the bearing, the measured variation in radial clearance can be as much as 25% as may be seen from Fig. 10. It was shown in Fig. 12 that if the resulting nips between the journal and the bearing lands are convergent with a T.I.R. of 25%, hydrodynamic pressures are generated with peak values that may be twice as large as the corresponding pocket pressure. These peak pressures will decrease with decreasing rotational velocity of the journal.
2. Circulatory flow of lubricant occurs in the pockets and, to a lesser

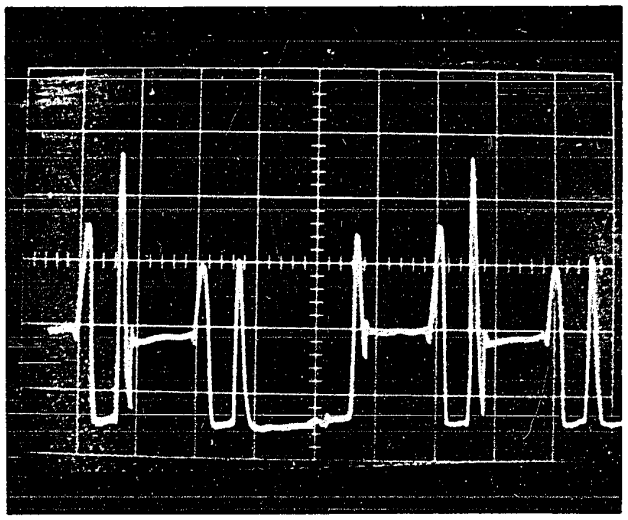

(a)

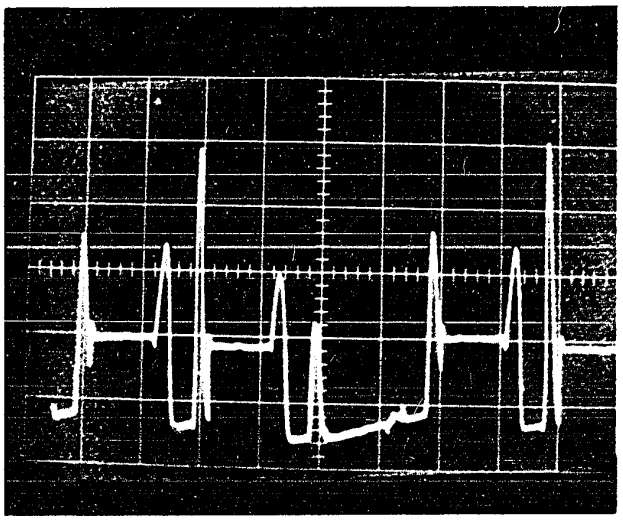

(b)

FIG. 27

(a) upper, (b) lower, are circumferential pressure profiles measured in the central diametral plane of the bearing. The pocket pressure is 90 p.s.i.g. (bearing load = 1000 lbs.). The journal speed is 1000 and 500 r.p.m. for Figs. (a) and (b) respectively. The ordinate scale is 46.7 p.s.i.g./cm in both cases and the abcissa is 20 ms/cm for Fig. (a) and 10 ms/cm for Fig. (b).

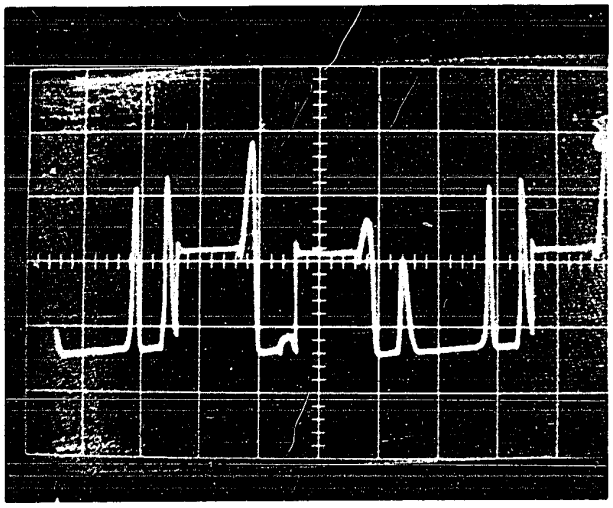

(a)

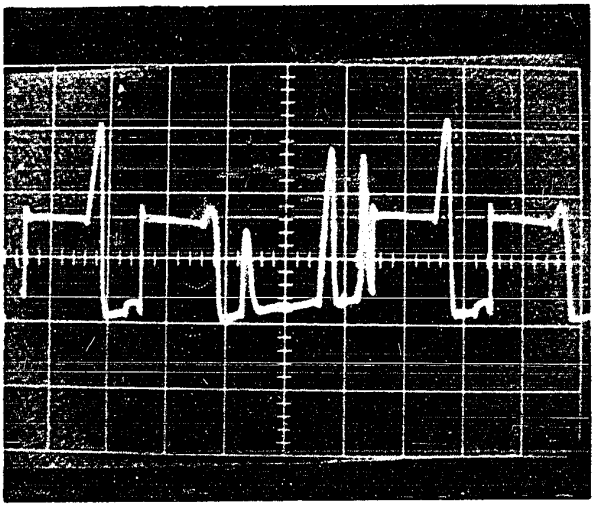

(b)

FIG. 28

(a) upper, (b) lower, are circumferential pressure profiles measured in the central diametral plane of the bearing. The pocket pressure is 180 p.s.i.g. (bearing load = 2000 lbs.). The journal speed is 1000 and 500 r.p.m. for Figs. (a) and (b) respectively. The ordinate scale is 93.4 p.s.i.g./cm in both cases and the abcissa is 20 ms/cm for Fig. (a) and 10 ms/cm for Fig. (b).

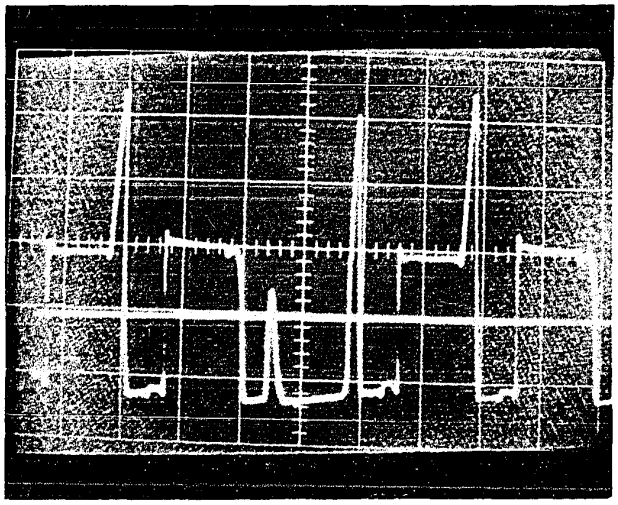

(a)

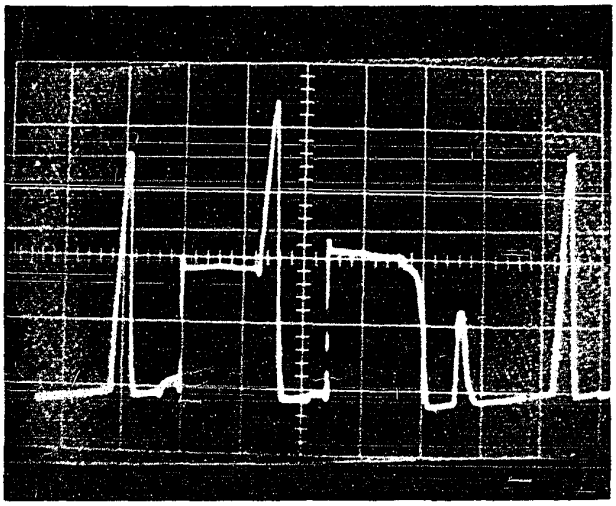

(b)

FIG. 29

(a) upper, (b) lower, are circumferential pressure profiles measured in the central diametral plane of the bearing. The pocket pressure is 250 p.s.i.g. (bearing load = 3000 lbs.). The journal speed is 1000 and 400 r.p.m. for Figs. (a) and (b) respectively. The ordinate scale is 93.4 p.s.i.g./cm in both cases and the abcissa is 20 ms/cm for Fig. (a) and 10 ms/cm for Fig. (b).

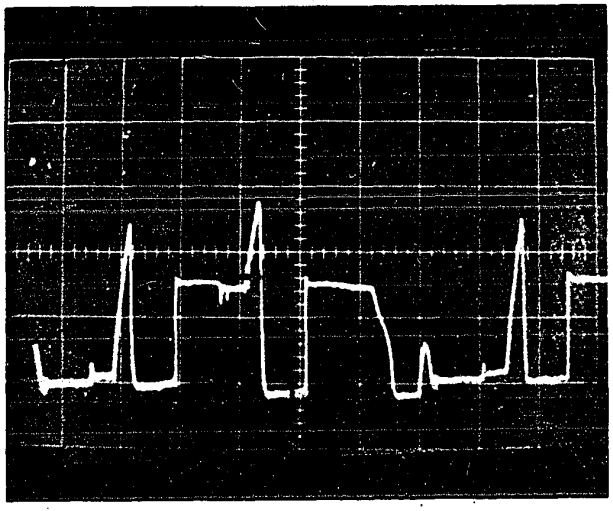

(a)

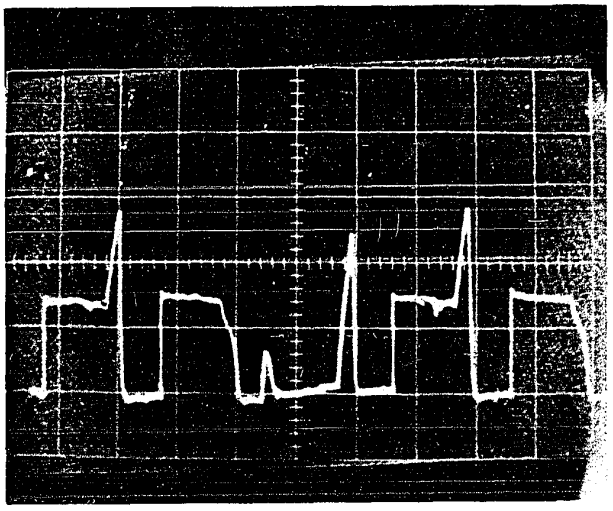

(b)

FIG. 30

(a) upper, (b) lower, are circumferential pressure profiles measured in the central diametral plane of the bearing. The pocket pressure is 380 p.s.i.g. (bearing load = 4000 lbs.). The journal speed is 900 and 200 r.p.m. for Figs. (a) and (b) respectively. The ordinate scale is 186.8 p.s.i.g./cm in both cases and the abcissa is 20 ms/cm for Fig. (a) and 10 ms/cm for Fig. (b).

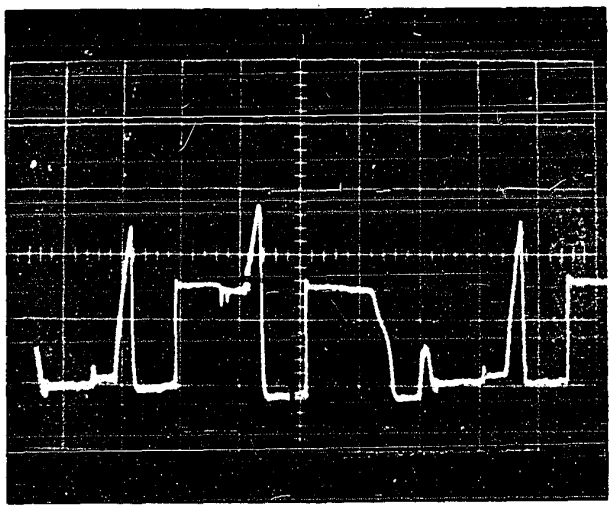

(a)

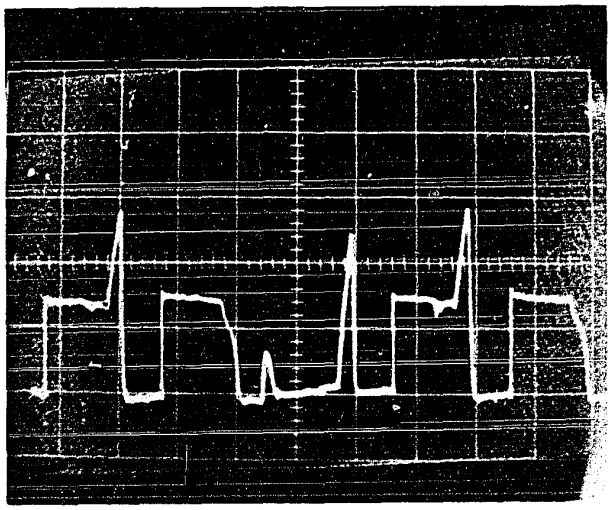

(b)

FIG. 30

(a) upper, (b) lower, are circumferential pressure profiles measured in the central diametral plane of the bearing. The pocket pressure is 380 p.s.i.g. (bearing load = 4000 lbs.). The journal speed is 900 and 200 r.p.m. for Figs. (a) and (b) respectively. The ordinate scale is 186.8 p.s.i.g./cm in both cases and the abcissa is 20 ms/cm for Fig. (a) and 10 ms/cm for Fig. (b).

extent, in the axial reliefs. This flow results from pressure gradients set up in these regions in the direction of rotation due to the step-bearing effect previously described. The magnitude of the pressure gradient along the pocket due to the presence of the step, may be calculated from equation (37). From the equation it is seen that the value of the gradient is a linear function of journal speed and is independent of pocket pressure. Fig. 31 is a plot of the pressure gradient predicted by this equation as a function of journal speed for the test bearing, assuming the temperature of the lubricant to be 100°F. At the highest journal speed, 1000 r.p.m., the predicted pressure gradient along the length of the pocket is 10 p.s.i.

Inertia forces associated with reversal of the flow direction of the circulating lubricant will give rise to a small negative pressure spike at the entrance to, and a small positive spike at the exit from, each pocket and axial relief. These spikes will be most noticeable at high rotational velocities of the journal and low pocket pressures. Increasing the pocket pressure at constant journal speed, and hence the hydrostatic flow component relative to the circulatory flow component, will reduce the size of the pressure spikes.

3. Lubricant flow conditions over the two axial lands adjacent to any pocket are generally different. The pressure gradient over either land is composed of three components: a linear gradient resulting from the hydrostatic pressure difference between the pocket pressure and the pressure in the adjacent axial relief, a smaller linear gradient resulting from the hydrostatic pressure difference between the pressure generated by the step in the axial relief prior to the entrance land and the pocket,

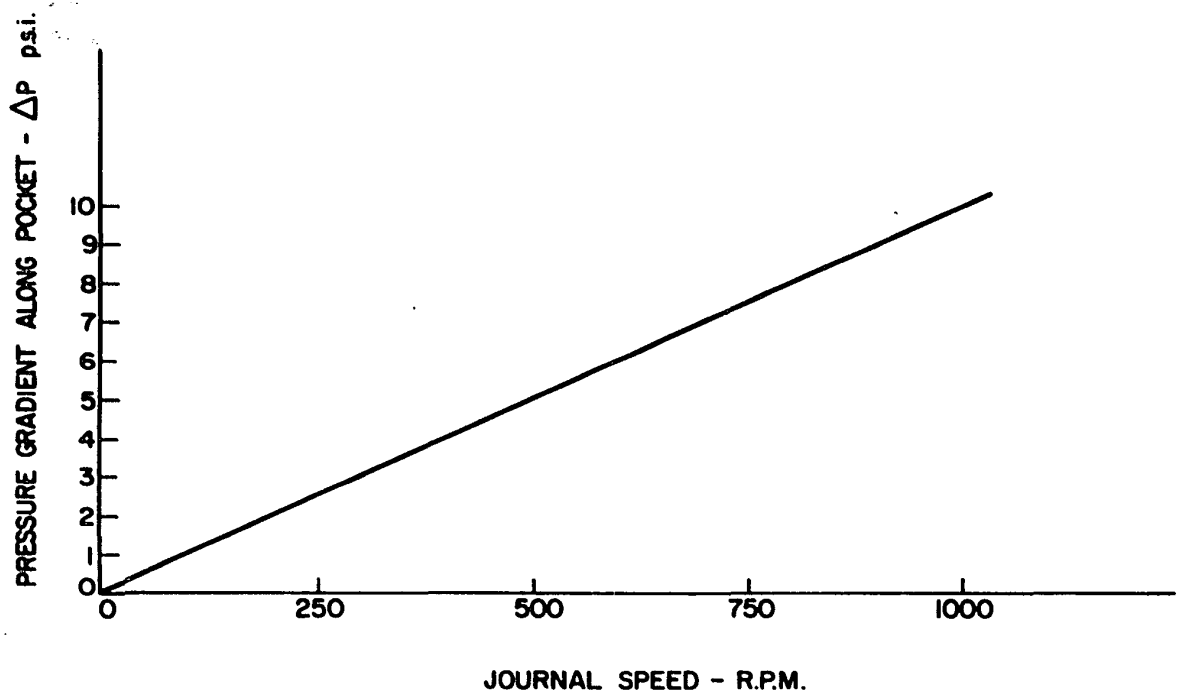

FIG. 31

Pressure gradient set up in pocket, as a result of the step bearing effect, as a function of journal speed. This gradient gives rise to lubricant circulation in the pocket.

or alternatively between the pressure generated by the step in the pocket prior to the exit land and that in the adjacent axial relief and finally any hydrodynamic pressure gradient arising from machine tolerances. The exact magnitude of the latter contribution at each land cannot be predicted with any degree of certainty since the geometry of the converging nip under the running conditions is not known. However, it may be observed that, as a useful corollary, the geometry of the nip may be estimated from the size of the measured pressure peak.

The flows associated with these components are in the same direction over the exit land, whereas over the entrance land the direction of flow associated with the first and second components are opposed. Hence, the flow rate over the exit land is always greater than that over the entrance land. In fact, the flow pattern over the entrance land can be complex and the direction and amount of the net flow over this land is determined by the relative values of the rotational velocity of the journal and the pocket pressure.

If there is a net flow out of the pocket over the land the lubricant is accelerated owing to the constriction in the flow path, and this will give rise to a pressure drop, or head loss, due to a Bernoulli effect at the entrance and exit steps of the pocket. Constantinescu (19) has recently shown that inertia forces associated with the acceleration of lubricant over such a step can often be quite significant.

In the light of these three additional effects it is now possible to describe in detail a typical measured profile. Fig. 32 shows a copied enlargement of the profile obtained at a pocket pressure of 90 p.s.i.g.

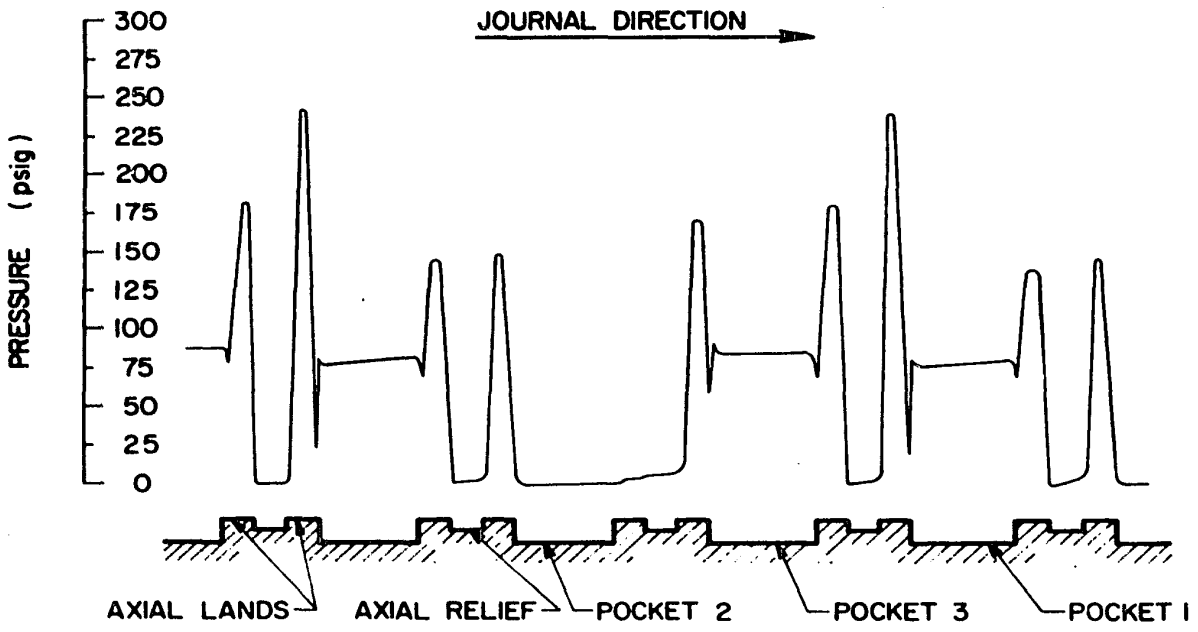

FIG. 32

Pressure profile in the lubricant film, measured in the central diametral plane of the bearing at 1000 r.p.m. and 1000 lb. loading, superimposed on the developed bearing profile.

and a journal speed of 1000 r.p.m. superimposed on the developed bearing configuration.

Starting at the left-hand side of the figure, it is seen that a large positive pressure peak extends over the full length of the entrance land to pocket 1. The origin and magnitude of this peak is consistent with the presence of a convergent nip between the journal and the land as measured in the T.I.R. diagram shown in Fig. 10. The sharp negative spike at the interface between the exit of the land and the entrance to the pocket is most probably due to inertia effects. A contribution to the spike may also arise from a change in the geometry of the nip from convergence to divergence just before the end of the land due to a slightly chamfered edge. In a 360° journal bearing large decreases in pressure cannot be sustained in the divergent nip since cavitation normally occurs, but in the present instance where a divergent nip would contain lubricant at a pressure slightly lower than that in the pocket, but above atmospheric, a pressure drop could easily be sustained. Following this spike a constant positive pressure gradient extends over the full length of the pocket indicating the presence of circulation. This pressure gradient across the pocket is of the expected order of magnitude. At the pocket exit, the small negative spike results from the algebraic sum of the negative spikes due to head loss and the positive spike due to flow reversal. Pressure peaks over both lands between pockets 1 and 2 are consistent with the presence of convergent nips between these lands and the journal. In the axial relief between these lands the pressure drops substantially to atmospheric with some evidence

of circulation. This arises from the fact that although lubricant flow in the relief is predominantly axial a small amount of circulation may be expected in the central region and this would fall off rapidly toward the circumferential ends.

Pocket 2, which is not pressurized, apparently contains lubricant at a pressure slightly in excess of atmospheric. This lubricant must be carried over from the adjacent relief by shear flow, and circulate in the pocket. The absence of hydrodynamic pressure over the exit land indicates that this bearing land and the journal are concentric. Over the succeeding land there is evidence of a convergent nip. Circulatory flow occurs in the axial relief between these two lands.

The profile in pocket 3 is qualitatively similar in all respects to that in pocket 1. However, it will be noted that the pressure in pocket 3 is somewhat higher than that in pocket 1 due to the individual adjustment of the pressures in these two pockets required to maintain the journal centrally located in the bearing. This higher pressure will tend to reduce the circulatory flow component relative to that in pocket 1 but the magnitude of the actual pressure gradient across pocket 3 is, for some unknown reason, somewhat less than that expected though the reduced circulation does to some extent account for the changes in the relative magnitude of the negative pressure spikes between the pockets 1 and 3. Both spikes appear to occur just inside the pocket, and if so the origin of the major component is unknown.

The trends in the profiles, shown in Figs. 27-30, are explicable in terms of the effects described above. Certain expected features are apparent.

For instance, the pressure gradients along the pockets are found to decrease with decreasing rotational velocity of the journal at a given load. As these gradients decrease, the size of the pressure spikes due to reversal of lubricant flow also decrease, leading to a smaller negative spike at the entrance to, and a larger negative spike at the exit from, the pocket.

Increasing the load, or pocket pressure, at constant r.p.m. produces a similar effect owing to the increased hydrostatic flow component. In the 3000 and 4000 lb. load tests the pressure gradients in the pocket appear to be negative. Actually, the circulatory flow component at these loads is so small that the pressure along the length of the pocket may be considered to be constant. The piezoelectric pressure sensor characteristically leaks charge when there is no change in pressure and therefore the signal drops off.

Hydrodynamic peak pressures over the axial lands should, at constant load, show a linear variation with rotational velocity. Cursory examination of pressure profiles obtained at equal pocket pressure and different rotational velocities shows that the variation of the size of the pressure peaks with r.p.m. is not as large as expected. For example, Fig. 28 shows pressure profiles around the bearing obtained at a pocket pressure of 180 p.s.i.g. for journal velocities of 1000 and 500 r.p.m. The peak pressure over the exit land of pocket 3 is only 12% less at 500 r.p.m. than at 1000 r.p.m. whereas a 50% reduction would have been expected. This apparent discrepancy arises from the fact that the average film temperatures during the two tests were not the same, hence the two measured profiles refer to pressure measurements in films of different

viscosity. Strict comparison of such profiles for the effect of journal speed requires that the measured peak pressures be corrected to equivalent film viscosity, from a knowledge of the average film temperature and the viscosity-temperature behaviour of the lubricant. A comparison of calculated and measured reductions in peak pressures over a range of loads and speeds corrected to equivalent lubricant viscosity at 100°F is given in the following table:

Load lb.	Percentage Reduction of Speed from 1000 r.p.m.	Percentage Reduction of Pressure Peak	
		Calculated	Measured
1000	50	50	41.5
2000	50	50	41
3000	50	50	42.5
4000	70	70	55

The agreement between measured and calculated values is quite good.

There is a noticeable difference between the pressure profiles of the 3000 and 4000 lb. load tests and those of the 1000 and 2000 lb. tests insofar as some of the hydrodynamic peaks have disappeared in the high load tests.

Examination of any one of the pressure profiles obtained at 3000-4000 lb. shows that over the entrance land to pocket 1 the pressure is zero indicating the presence of a divergent nip in the lubricant film, whereas over the exit land the pressure profile is close to the Laplacian prediction indicating that the surfaces of the land and journal are parallel. The profile in pocket 2 has not changed qualitatively from the lighter load tests although the magnitude of the hydrodynamic peaks has

changed. Pocket No.3 shows a suppression of the pressure over the entrance land similar to that at the entrance to pocket 1 but a hydrodynamic peak occurs over the exit land.

It is possible that a slight amount of wear which occurred in the bearing prior to the higher load tests was responsible for these changes.

Friction Torque

Friction torque was measured at selected combinations of journal speed and load through a range of journal speeds of 100-1000 r.p.m. and loads of 1000-4000 lb.

Owing to the inadequacy of the cooling system in the lubricant supply unit it was not possible to maintain the average film temperature of the lubricant at an arbitrary standard value for all combinations of values of journal speed and load employed in the tests. Therefore, the measured values of friction torque were corrected to an average film temperature of 100°F in order that a comparison of experimental and theoretical values could be made. The average film temperature recorded is the mean of the measured temperatures of the lubricant into and out of the bearing.

From equation (45), friction torque is related to temperature solely through the viscosity, being directly proportional to the viscosity. The torque at 100°F is:

$$T(100) = \frac{\mu(100)}{\mu(x)} \times T(x)$$

where $T(x)$ is the measured torque at an average film temperature of x°F. The adjusted torques are given in Table I. Fig. 33 is a plot of friction

TABLE 1

Load lb.	R.P.M.	Average Temperature °F	Viscosity x 10^{-6} lb. - sec/in^2	Torque (100°F) in. - lb.
1000	1000	108.5	11.7	115.2
	900	109.0	11.5	147.0
	800	108.5	11.7	139.0
	700	107.5	12.0	113.0
	600	106.0	12.5	101.5
	500	104.0	13.2	83.0
	400	103.0	13.6	68.2
	300	102.0	14.1	61.0
2000	1000	104	13.4	195
	900	105	13.0	193
	800	105.5	12.8	189
	700	104.0	13.4	162
	600	103.0	13.8	150
	500	101.0	14.5	134
	400	99.0	15.5	119
	300	97.0	16.8	99.5
	200	94.0	18.4	71.0
	100	92.0	19.8	57.2
3000	1000	111.0	10.7	276
	900	110.5	10.8	264
	800	109.0	11.3	230
	700	108.0	11.8	234
	600	106.5	12.2	213
4000	1000	115.0	9.5	346
	900	115.0	9.5	365
	800	114.0	9.8	338
	700	112.0	10.4	307
	600	109.5	11.2	262
	500	107.5	12.0	238
	400	105.5	13.0	215
	300	103.0	13.7	192

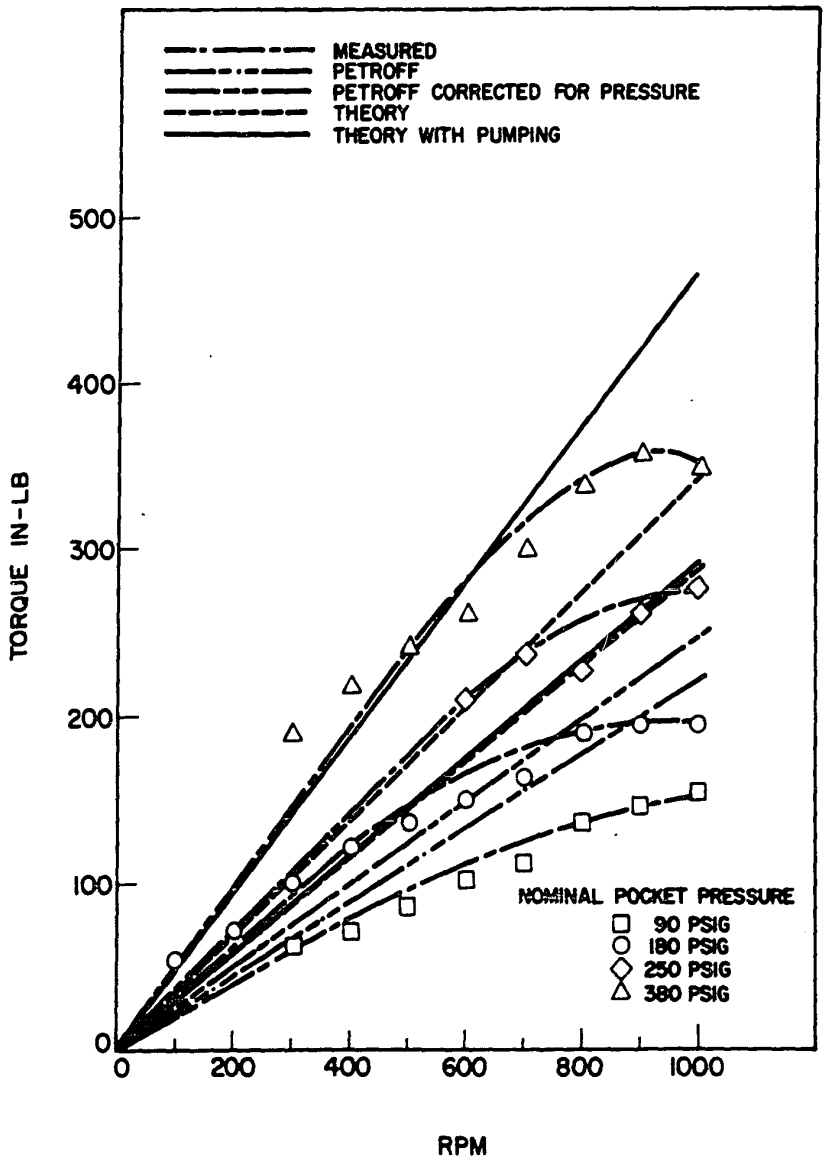

FIG. 33

Measured friction torque vs. journal speed at four pocket pressures for the test bearing. The following theoretically predicted curves are also shown. A prediction according to Petroff's equation for friction torque, and the range of Petroff predictions using a correction for viscosity dependence on pressure. A prediction for friction torque allowing for pocket friction and the range of friction torque with the pressure-viscosity correction. A prediction which includes an estimate for pumping lubricant over the lands.

torque corrected to 100°F as a function of journal speed at various pocket pressures.

The same plot shows two predictions of friction torque, according to Petroff's equation, through the range of journal speeds used. The lower Petroff curve predicts the friction torque due to shear over the land areas only, according to equation (42), for the lowest pocket pressure used during the tests. The average film temperature for this calculation is assumed to be 100°F. The higher Petroff curve takes into account the influence of pressure on lubricant viscosity and predicts friction torque as before for a pressure of 380 p.s.i.g., the highest pocket pressure used during the tests. The average film temperature is again assumed to be 100°F.

Friction torque is then calculated according to equation (45) which takes into account the friction loss in the pockets. Predicted values also include a pressure - viscosity correction and curves are given for pocket pressures of 90 and 380 p.s.i.g. Calculations are based on an average film temperature of 100°F. Since equation (45) accounts for the friction loss in the pocket the lubricant temperature in the pocket must be derived from equation (52), where it is assumed that the average film temperature is 100°F.

Comparison of the two predictions of friction torque shows that the friction loss in the pocket is quite significant, being approximately 27% and 38% of the land friction losses as predicted by the Petroff equation, at pocket pressures of 90 and 380 p.s.i.g. respectively. The difference between the two predictions is independent of journal speed as equations (42) and (45) indicate. However, the difference depends

on pocket pressure since the latter is implicitly defined in the viscosity term. These results are in close agreement with those obtained by Shinkle and Hornung (8).

Even after making allowance for friction loss in the pockets and the effect of pressure on lubricant viscosity, the variation of friction torque with pocket pressure is greater than that predicted by this theory.

Part of the reason for this unpredicted dependence of friction torque on pocket pressure can be explained by reference to the measured pressure profiles. The hydrodynamic pressure peaks over the axial lands are adverse pressure gradients which the normal circumferential flow of fluid, caused by journal rotation, must overcome. Flow of fluid through these high pressure regions is promoted by a pumping action and the work involved in the pumping must come from the shaft and hence it contributes to the friction torque.

The order of magnitude of this pumping work can be found by multiplying the peak pressure by the corresponding flow rate of lubricant over the land areas. If this quantity is then equated to the product of a force tangential to the journal surface and the peripheral journal speed

$$\sum_{\text{Land}} P \times Q = F \times V$$

the torque, T_p, resulting from the pumping is

$$T_p = F \times R = \frac{\sum_{\text{Land}} (P \times Q) \times R}{V}$$

The torque due to the pumping work when added to the theoretical prediction

for the pocket pressure of 380 p.s.i.g. should form an upper limit for the measured torques. This is seen to be so.

It will, of course, be noted that the size of this correction will vary with the dimensional tolerance as well as with the operational parameters of the bearing.

It is also seen that the measured torque data for each pressure appear to increase at a decreasing rate with increasing journal speed. A common assumption made when modelling the dynamics of film lubrication is to consider that the lubricant temperature across the film is constant. Hagg (15) has shown that for a journal bearing running at zero eccentricity there is a temperature variation across the film which must also be reflected in a variation of film viscosity. In turn, this variation of viscosity affects the velocity distribution and thus the shear. Such an analysis for the configuration of bearing used in this work was not attempted due to the complexity of the problem. However, Fig. 34 shows the qualitative effect on torque with journal speed, when Hagg's prediction is compared to Petroff's prediction for a concentrically running journal bearing with a film area equal to that of the test bearing.

There is a marked decrease in predicted torque from the Petroff prediction as the journal speed increases. Thus, it is postulated that the decrease in torque from the Petroff prediction at higher journal speeds is due to the radial variation of lubricant temperature across the lubricant film.

Minimum Torque

During the course of the experimental investigation it was found,

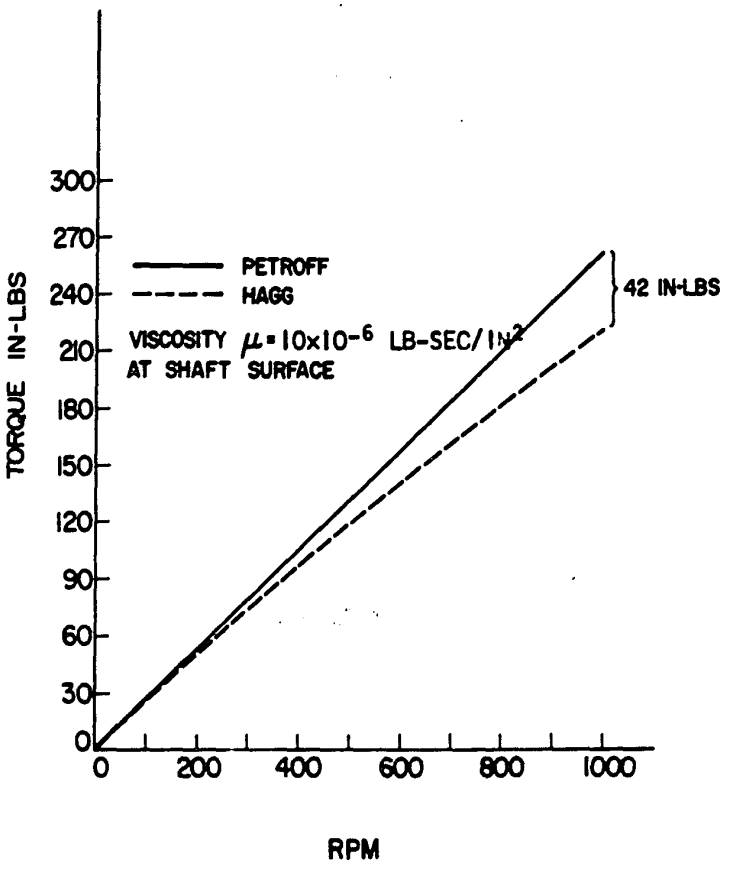

FIG. 34

Friction torque loss vs. journal speed illustrating the difference between the predictions of Petroff and Hagg for a concentrically running journal bearing of the same bearing area as the hydrostatic bearing used in this study.

quite unexpectedly, that the friction torque fell to about 40-50 percent of its value at zero eccentricity by allowing the journal to adopt an eccentric position.

This was achieved by systematically lowering the hydrostatic pressure to pockets 1 and 3 by the following procedure. The journal was rotated at 1000 r.p.m. and brought to a position of zero eccentricity and the temperature allowed to equilibrate. The pressures in pockets 1 and 3 were then adjusted so that the journal took up a position of minimum torque.

Results for some of these tests, which cannot be regarded as exhaustive and require further investigation, are shown in Table 2. It would appear that the friction torque may be reduced by as much as 40 percent from the value at zero eccentricity by slowly decreasing the pressures in pockets 1 and 3 to zero and allowing the journal to approach a position of unit eccentricity. Though the torque can be substantially reduced, operation under these conditions is neither stable nor to be recommended since it involves continuous change of direction of application of the external load which would ultimately lead to contact between the journal and bearing, and possible seizure.

It is fully recognized that this somewhat surprising result requires further investigation, particularly the measurement of the relevant pressure profiles and a complete theoretical consideration of eccentric operation. For this reason there was some hesitation regarding its inclusion in this thesis. However, it is a real result obtained on a real bearing and, whatever reason lies behind its explanation, it was felt that some mention of it should be made.

TABLE 2

Minimum Torque

Load lb.	Torque + Starting Friction in.lb.	Torque - Starting Friction in.lb.	Torque in.lb	Eccentricity (x,y)	% Reduction of Torque
1000	205	167	186	(0,0)	
	159	139	149	(.75,.4)	20%
2000	227	156	191	(0,0)	
	155	128	141	(1,.25)	26%
3000	258	200	229	(0,0)	
	161	123	142	(.95,.05)	38%
4000	280	205	242	(0,0)	
	166	133	149	(1.0)	38.5%

Temperature Change Through Bearing

Measurements of the temperature change of the lubricant as it passes through the bearing, as a function of journal speed through the range 200-1000 r.p.m., at pocket pressures of 150, 280 and 400 p.s.i.g., are presented in Table 3 and graphically in Fig. 35.

The three sets of points given for each pressure represent:-

1) The measured difference between the temperature of the lubricant entering and leaving the bearing.

2) Calculated differences using a viscosity based on the average of the inlet and outlet temperatures of the lubricant ignoring the fluid dynamics in the pocket. The inlet temperature is the measured inlet temperature and the outlet temperature is found by an iterative solution of the heat balance equations (47) and (49). These are shown under calculation 1 in Table 3.

3) Calculated differences using a viscosity corrected for pressure. The viscosity is based on the inlet temperature to the film for the term in equation (52) that applies to the pocket, and on the average of the inlet and outlet temperature of the film for those terms in equation (52) that apply to the land areas. The inlet temperature to the bearing is the measured value and the outlet temperature is found by an iterative solution of equation (52). These are shown under calculation 2 in Table 3.

In general, the average film temperature of the bearing is taken

TABLE 3

Pocket Pressure 150 p.s.i.g.				Pocket Pressure 280 p.s.i.g.				Pocket Pressure 400 p.s.i.g.			
ΔT °F / RPM	Meas.	Calc.I	Calc.2	ΔT °F / RPM	Meas.	Calc.I	Calc.2	ΔT °F / RPM	Meas.	Calc.I	Calc.2
1000	40.0	76.0	49.0	1000	38.5	54.0	38.0	1000	28.0	26.0	24.0
750	35.0	64.0	42.0	650	33.0	44.0	31.5	750	24.0	30.0	25.0
500	27.5	48.0	32.0	500	28.0	30.0	25.0	500	22.0	24.0	21.0
250	14.5	2.0	20.0	300	21.0	18.0	16.5	250	14.0	12.0	14.0

Measured and calculated temperature change of lubricant through the bearing as a function of pocket pressure and journal speed.

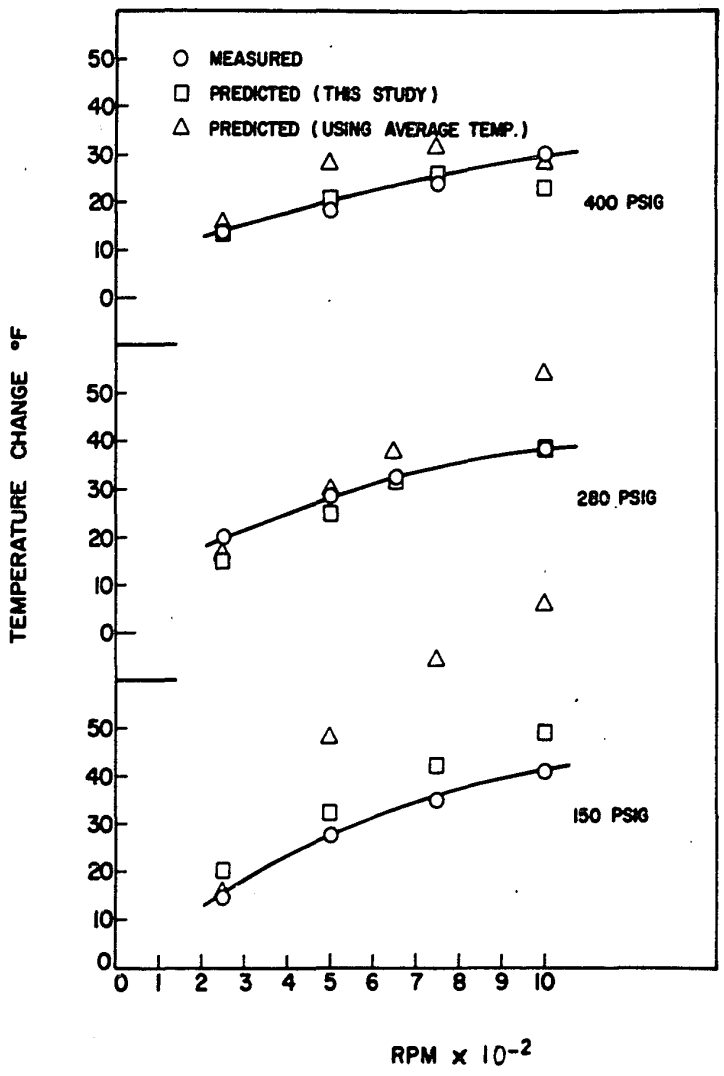

FIG. 35

Measured and predicted values of the increase in lubricant temperature as it passes through the bearing.

as the average of the measured inlet and outlet temperatures of the lubricant. This assumption is a good one when the shaft speed is low or the hydrostatic pressure is very large. As circulatory flow in the pocket increases, lubricant entering the pocket is subjected to a significant amount of shear before entering the bearing film. This raises the temperature of the lubricant entering the bearing film to a value above the inlet temperature to the pocket and results in an average lubricant temperature in the bearing film which is higher the average of the inlet and outlet temperatures.

Referring to Fig. 35, it can be seen that the calculated value of the temperature rise through the bearing based on the average of the inlet and outlet temperatures is in very poor agreement in the low pressure test. In this case the circulatory flow component accounts for 90% of the flow in the pocket and the temperature rise of the lubricant in the pocket alone is 28°F. The prediction improves considerably in the higher pressure tests where the flow in the pocket becomes more hydrostatic in nature.

The theoretical prediction accounting for both circulatory flow and pressure-viscosity dependence is in much better agreement with the measured values. The theoretical predictions for the 150 p.s.i.g. test are consistently higher than the measured values while those for the 280 and 400 p.s.i.g. tests fall a little below the measured data.

These discrepancies are believed to be due to two separate phenomena. First, a quantity of heat is absorbed by the lubricant film owing to the pumping action, discussed previously, which has not been allowed for in the calculation. Values of the measured exhaust

temperature can be adjusted to allow for the temperature increase due to the pumping action. Calculations show that rises of 4°F and 1°F would be expected at 400 and 150 p.s.i.g. respectively. If these quantities are subtracted from the respective measured values of temperature rise to obtain adjusted values for no pumping the discrepancies, in general become positive, the overall discrepancy being larger at lower pressure.

Secondly, the calculations of lubricant temperature rise do not allow for transfer of heat from the lubricant to the bearing members. Thus, the calculated values of temperature rise would be higher than the measured values since it is assumed that all the heat developed in the lubricant remains in the lubricant as it leaves the bearing. Differences between measured and calculated values, as seen in Fig. 35, may be explained qualitatively on this account. Relatively more heat is transferred from the lubricant to the bearing member at lower pocket pressure owing to the longer dwell time of the lubricant in the bearing. Thus, the divergence between the calculated and measured values should be greater at lower pocket pressure as is found.

CONCLUSIONS

The main conclusion to be drawn from this study is that the practical behaviour of a hydrostatic journal bearing, designed to carry loads of up to 4000 lb. at journal speeds of up to 1000 r.p.m. and machined according to standard machine tolerances of ± 0.0001in., shows a marked discrepancy from that predicted by existing theory.

An analysis of the origin of these discrepancies has been enormously facilitated by the experimental measurement of the fluid pressure distribution in the bearing, a measurement which has never before been made.

It may be remarked that machining to closer tolerances, such as is demanded in the manufacture of gas bearings where tolerances are held to 0.1% of the film thickness, would eliminate much of the discrepancy as would operation at increased radial clearance. From a practical viewpoint, however, where one might have to assess the relative economics of different types of bearing for operation under the conditions described, which pertain to the requirements of most industrial machinery, more sophisticated machining techniques and the necessity for larger capacity lubricant supply systems required for operation at increased radial clearance, would probably be unattractive. Each possible application would have to be judged on its own merits.

The importance of a quantitative knowledge of the temperature distribution of the lubricant in the bearing cannot be overstressed. Present methods of assessment of this factor are quite inadequate and lead to large errors in the estimation of friction torque.

Consideration of the various alternatives which would give a preferred solution to the problem which led to this study, leaves little doubt that the construction of a bearing in which the effect of machining tolerances are negligible would be best. The uncertainty of obtaining a satisfactory estimate of friction torque is obviously precluded by the quantitatively unpredictable effects of machining tolerance.

Certain improvements in the experimental arrangement could be suggested, as a result of this study, for consideration in any future work on this subject. These are listed later.

CLAIMS OF ORIGINAL CONTRIBUTION

1. A theoretical model for a high speed highly loaded hydrostatic bearing has been developed, which includes the influence of machining tolerances in the bearing on the circumferential pressure profile in the lubricant film. The model provides a satisfactory explanation of the experimentally measured pressure profiles.

2. A method of continuously monitoring the pressure profile around the bearing has been developed, the results of which show that the Laplacian prediction of pressure distribution for a nominally concentric operating position is wholly inadequate for the bearing tested.

3. A theoretical model of lubricant temperature change as it passes from the pocket source to the axial reliefs has been developed which allows for the effect of lubricant temperature change in the pocket due to lubricant dynamics there. This model adequately describes the total temperature rise of the lubricant as it passes through the bearing.

SUGGESTIONS FOR FURTHER WORK

1. The test bearing should be supported by and loaded through a second hydrostatic bearing to enable direct measurement of friction shear losses in the test bearing.

2. Allowance should be made for the test bearing to be moved in an axial direction during operation to enable complete mapping of the pressure field over the whole bearing pad.

3. Development of a technique of scanning the temperature distribution in the lubricant film.

4. Design of a system to control the temperature of the journal and bearing to facilitate an assessment of heat losses from the film to the bearing members.

BIBLIOGRAPHY

1. Zsombor-Murray, P.J.A., Ph.D. Thesis, Department of Mechanical Engineering, McGill University, June 1971.

2. Harris, T.A., Roller Bearing Analysis, John Wiley and Sons, Inc. New York, 1966.

3. Fuller, D.D., Machine Design, 19, (6); 110. 19, (7); 117. 19, (8); 115 (1947).

4. Fuller, D.D., Theory and Practice of Lubrication for Engineers, John Wiley and Sons, New York, 1956.

5. Rippel, H.C., Cast Bronze Hydrostatic Bearing Manual, Cast Bronze Bearing Institute Inc., Cleveland, 1965.

6. Royle, J.K., Howarth R.B. and Caseley-Hayford, A.L., Proc. Instn. Mech. Eng., 176, (22); 532-41 (1962).

7. Michell, A.G.M., Lubrication, Blackie and Son Limited, London and Glasgow, 1950.

8. Shinkle, J.N. and Hornung, K.G., Journal of Basic Engineering, 87, (1); 163 (1965).

9. Raimondi, A.A. and Boyd, S., Lubrication Eng., 13, 28 (1957).

10. O'Donoghue, S.P. and Rowe, W.P., Tribology, 1, (4); 230 (1968).

11. Dickson, S.L., U.K. Atomic Energy Authority, IGR-Tn/CA-768, October 1967.

12. Kher, A.K. and Cowley, A., Tribology, 3, 165 (1970).

13. Bradford, L.J. and Villforth, F.J. Jr., A.S.M.E. Trans. 63, 359-362 (1941).

14. Cole, J.A. Proceedings of the Conference on Lubrication and Wear, The Institution of Mechanical Engineers, London, 1957, pp.111.

15. Hagg, A.E., Trans. A.S.M.E., 66, A.72 (1944).

16. Muskat, M. and Morgan, F., Jour. Appl. Phys. 14, 234 (1943).

17. Constantinescu, V.N., Journal of Lubrication Technology, 92, Series F, (3); 473 (1970).

APPENDIX I

COMPUTER PROGRAMS

```
FORTRAN IV G LEVEL 1, MOD 3    MAIN     DATE = 69080          13/52/08

0001      DIMENSION A(21,27)
      C   SOLUTION TO LAPLACES EQUATION FOR RECTANGLUAR PAD %DEVELOPED<
0002      READ(5,1)((A(I,J),J=1,27),I=1,21)
0003    1 FORMAT(16F5.0/11F5.0)
0004      KOUNT=0
0005      ALFA=1.6/4.
0006      E=0.2
0007      F=0.5
0008   11 BIGEST=0.
0009      DO 7 I=2,20
0010      IF(I.GE.6)GO TO 2
0011      MIN=2
0012      RES=2.*A(I,2)+A(I-1,1)+A(I+1,1)-4.*A(I,1)
0013      BIGEST=AMAX1(BIGEST,ABS(RES))
0014      A(I,1)=A(I,1)+ALFA*RES
0015    3 DO 8 J=MIN,25
0016      RES=A(I,J+1)+A(I,J-1)+A(I+1,J)+A(I-1,J)-4.*A(I,J)
0017      BIGEST=AMAX1(BIGEST,ABS(RES))
0018    8 A(I,J)=A(I,J)+ALFA*RES
0019      RES1=2.*A(I,27)/(E*(1.+E))+2.*A(I,25)/(1.+E)+A(I-1,26)+A(I+1,26)
0020      RES2=2.*(1.+1./E)*A(I,26)
0021      RES=RES1-RES2
0022      BIGEST=AMAX1(BIGEST,ABS(RES))
0023      A(I,26)=A(I,26)+ALFA*RES/(1.+1./E)
0024      GO TO 7
0025    2 MIN=17
0026      DO 17 J=MIN,26
0027      IF(J-17)5,6,5
0028    6 RES1=2.*A(I,16)/(F*(1.+F))+2.*A(I,13)/(1.+F)+A(I-1,17)+A(I+1,17)
0029      RES2=2.*(1.+1./F)*A(I,17)
0030      RES=RES1-RES2
0031      BIGEST=AMAX1(BIGEST,ABS(RES))
0032      A(I,17)=A(I,17)+ALFA*RES/(1.+1./F)
0033      GO TO 17
0034    5 IF(J-26)9,10,9
0035   10 RES1=2.*A(I,27)/(E*(1.+E))+2.*A(I,25)/(1.+E)+A(I-1,26)+A(I+1,26)
0036      RES2=2.*(1.+1./E)*A(I,26)
0037      RES=RES1-RES2
0038      BIGEST=AMAX1(BIGEST,ABS(RES))
0039      A(I,26)=A(I,26)+ALFA*RES/(1.+1./E)
0040      GO TO 17
0041    9 RES=A(I,J+1)+A(I,J-1)+A(I+1,J)+A(I-1,J)-4.*A(I,J)
0042      BIGEST=AMAX1(BIGEST,ABS(RES))
0043      A(I,J)=A(I,J)+ALFA*RES
0044   17 CONTINUE
0045    7 CONTINUE
0046      DO 15 J=17,26
0047      IF(J-17)18,18,19
0048   18 RES1=2.*A(21,16)/(F*(1.+F))+2.*A(21,13)/(1.+F)+2.*A(20,17)
0049      RES2=2.*(1.+1./F)*A(21,17)
0050      RES=RES1-RES2
0051      BIGEST=AMAX1(BIGEST,ABS(RES))
0052      A(21,17)=A(21,17)+ALFA*RES/(1.+1./F)
0053      GO TO 15
```

```
FORTRAN IV G LEVEL 1, MOD 3 MAIN  DATE = 69080          13/52/08

0054            19 IF(J-26)23,22,23
0055            22 RES1=2.*A(21,27)/(E*(1.+E))+2.*A(21,25)/(1.+E)
0056               RES2=2.*A(20,26)-2.*(1.+1./E)*A(21,26)
0057               RES=RES1+RES2
0058               BIGEST=AMAX1(BIGEST,ABS(RES))
0059               A(21,26)=A(21,26)+ALFA*RES/(1.+1./E)
0060               GO TO 15
0061            23 RES=2.*A(20,J)+A(21,J+1)+A(21,J-1)-4.*A(21,J)
0062               BIGEST=AMAX1(BIGEST,ABS(RES))
0063               A(21,J)=A(21,J)+ALFA*RES
0064            15 CONTINUE
0065               KOUNT=KOUNT+1
0066               IF(KOUNT.EQ.100)GO TO 30
0067               IF(BIGEST.GE.1.0)GO TO 11
0068            30 WRITE(6,12)((A(I,J),I=1,21),J=1,27)
0069            12 FORMAT(1H1,/(1H ,21F6.0/))
0070            34 WRITE(6,35)KOUNT
0071            35 FORMAT(1H1,10X,12HKOUNT EQUALS,2X,I5)
0072               WRITE(6,36)A(5,15),A(5,23),A(3,21),A(8,20),A(3,10)
0073            36 FORMAT(/,F10.3)
0074               STOP
0075               END

 TOTAL MEMORY REQUIREMENTS 00124E BYTES
```

```
FORTRAN IV G LEVEL 1, MOD 3   MAIN     DATE = 69071          17/22/51

0001        DIMENSION A(21,21)
      C     SOLUTION TO LAPLACES EQUATION FOR A RECTANGULAR BEARING PAD
0002        READ(5,1)((A(I,J),J=1,21),I=1,21)
0003      1 FORMAT(16F5.0/5F5.0)
0004        DO 4 I=2,8
0005        DO 4 J=2,20
0006        S1=A(I-1,J)+A(I,J-1)+A(I+1,J)+A(I,J+1)
0007        S2=A(I-1,J-1)+A(I+1,J-1)+A(I+1,J+1)+A(I-1,J+1)
0008        A(I,J)=(4*S1+S2)/20
0009      4 CONTINUE
0010        DO 5 I=9,20
0011        DO 5 J=17,20
0012        S1=A(I-1,J)+A(I,J-1)+A(I+1,J)+A(I,J+1)
0013        S2=A(I-1,J-1)+A(I+1,J-1)+A(I+1,J+1)+A(I-1,J+1)
0014        A(I,J)=(4*S1+S2)/20
0015      5 CONTINUE
0016        WRITE(6,15)((A(I,J),J=1,21),I=1,21)
0017     15 FORMAT(1X,21F6.0)
0018        KOUNT=0.
0019        ALFA=1.6/4.
0020     11 BIGEST=0.
0021        DO 9 I=2,20
0022        IF(I.GE.9)GO TO 2
0023        MIN=2
0024        RES=2.*A(I,2)+A(I-1,1)+A(I+1,1)-4.*A(I,1)
0025        BIGEST=AMAX1(BIGEST,ABS(RES))
0026        A(I,1)=A(I,1)+ALFA*RES
0027        GO TO 3
0028      2 MIN=17
0029      3 DO 8 J=MIN,20
0030        RES=A(I,J+1)+A(I,J-1)+A(I+1,J)+A(I-1,J)-4.*A(I,J)
0031        BIGEST=AMAX1(BIGEST,ABS(RES))
0032      8 A(I,J)=A(I,J)+ALFA*RES
0033        DO 7 J=17,20
0034        RES=2*A(20,J)+A(21,J-1)+A(21,J+1)-4.*A(21,J)
0035        BIGEST=AMAX1(BIGEST,ABS(RES))
0036      7 A(21,J)=A(21,J)+ALFA*RES
0037        KOUNT=KOUNT+1
0038        IF(KOUNT.EQ.100)GO TO 10
0039        IF(BIGEST.GE.1.0)GO TO 11
0040     10 WRITE(6,12)((A(I,J),J=1,21),I=1,21)
0041     12 FORMAT(1H1,/(1H ,21F6.0/))
0042        STOP
0043        END

 TOTAL MEMORY REQUIREMENTS 000CF6 BYTES
```